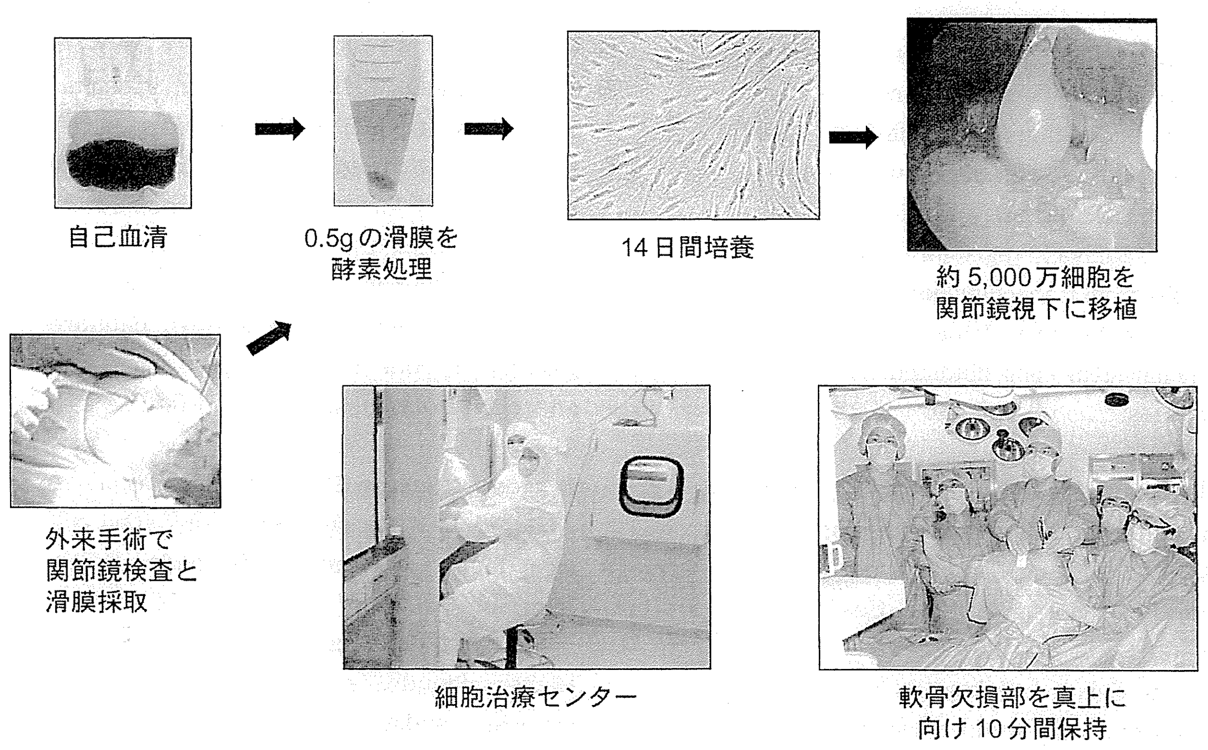

図 10　滑膜幹細胞を用いる低侵襲軟骨再生医療のスキーム

外来手術で関節鏡検査の際に滑膜を 0.5 g 採取し，細胞治療センターで酵素処理後，自己血清を用いて 14 日間培養し，約 5,000 万の滑膜幹細胞の浮遊液を関節鏡視下で軟骨欠損部に 10 分間静置し接着させる。
（筆者提供）

節鏡検査と同時に滑膜を採取する。本学の手術室と同じフロアにある細胞治療センターで，滑膜を酵素処理後，10%自己血清を用いて滑膜幹細胞を 14 日間培養する。平均 0.5 g の滑膜と 70 mL の自己血清から，14 日間で平均 5,000 万細胞を採取できる。この細胞の浮遊液を関節鏡視下で軟骨欠損部に 10 分間静置する（**図 10**）。後療法は，外固定をせず，2 週後から部分荷重，6 週後から全荷重を開始する。この方法は動物血清や人工素材を必要とせず，低侵襲で実施可能である利点がある。これまで重篤な副作用を認めていない。多数の例で軟骨欠損部の再生，症状の改善を認めている。本軟骨治療の真の有効性を判断するためには多数例の長期間にわたる観察が必要であると考えている。

文　献

1) Koga H, Engebretsen L, Brinchmann JE, et al : Mesenchymal stem cell-based therapy for cartilage repair : a review. Knee Surg Sports Traumatol Arthrosc **17** : 1289-1297, 2009.
2) Pittenger MF, Mackay AM, Beck SC, et al : Multilineage potential of adult human mesenchymal stem cells. Science **284** (5411) : 143-147, 1999.
3) Friedenstein AJ, Piatetzky S, II, Petrakova KV : Osteogenesis in transplants of bone marrow cells. J Embryol Exp Morphol **16** (3) : 381-390, 1966.
4) Segawa Y, Muneta T, Makino H, et al : Mesenchymal stem cells derived from synovium, meniscus, anterior cruciate ligament, and articular chondrocytes share similar gene expression profiles. J Orthop Res **27** (4) : 435-441,

2009.
5) Sekiya I, Larson BL, Smith JR, et al : Expansion of human adult stem cells from bone marrow stroma : conditions that maximize the yields of early progenitors and evaluate their quality. Stem Cells **20** (6) : 530-541, 2002.
6) Sakaguchi Y, Sekiya I, Yagishita K, et al : Suspended cells from trabecular bone by collagenase digestion become virtually identical to mesenchymal stem cells obtained from marrow aspirates. Blood **104** (9) : 2728-2735, 2004.
7) Sekiya I, Larson BL, Vuoristo JT, et al : Comparison of effect of BMP-2, -4, and -6 on in vitro cartilage formation of human adult stem cells from bone marrow stroma. Cell Tissue Res **320** (2) : 269-276, 2005.
8) Shirasawa S, Sekiya I, Sakaguchi Y, et al : In vitro chondrogenesis of human synovium-derived mesenchymal stem cells : Optimal condition and comparison with bone marrow-derived cells. J Cell Biochem **97** (1) : 84-97, 2006.
9) Sekiya I, Vuoristo JT, Larson BL, et al : In vitro cartilage formation by human adult stem cells from bone marrow stroma defines the sequence of cellular and molecular events during chondrogenesis. Proc Natl Acad Sci U S A **99** (7) : 4397-4402, 2002.
10) Nagase T, Muneta T, Ju YJ, et al : Analysis of harvest sites and culture parameters for optimal in vitro chondrogenic potential of synovial mesenchymal stem cells from knee joints with medial compartment osteoarthritis. Arthritis Rheum **58** (5) : 1389-1398, 2008.
11) Sakaguchi Y, Sekiya I, Yagishita K, et al : Comparison of human stem cells derived from various mesenchymal tissues : Superiority of synovium as a cell source. Arthritis Rheum **52** (8) : 2521-2529, 2005.
12) Yoshimura H, Muneta T, Nimura A, et al : Comparison of rat mesenchymal stem cells derived from bone marrow, synovium, periosteum, adipose tissue, and muscle. Cell Tissue Res **327** (3) : 449-462, 2007.
13) Koga H, Muneta T, Nagase T, et al : Comparison of mesenchymal tissues-derived stem cells for in vivo chondrogenesis ; Suitable condition of cell therapy for rabbit cartilage defects Cell Tissue Res **333** (2) : 207-215, 2008.
14) Ichinose S, Muneta T, Koga H, et al : Morphological differences during in vitro chondrogenesis of bone marrow-, synovium-MSCs, and chondrocytes. Lab Invest **90** (2) : 210-221, 2010.
15) Dragoo JL, Samimi B, Zhu M, et al : Tissue-engineered cartilage and bone using stem cells from human infrapatellar fat pads. J Bone Joint Surg Br **85** (5) : 740-747, 2003.
16) Mochizuki T, Muneta T, Sakaguchi Y, et al : Higher chondrogenic potential of fibrous synovium- and adipose synovium-derived cells compared with subcutaneous fat-derived cells: distinguishing properties of mesenchymal stem cells in humans. Arthritis Rheum **54** (3) : 843-853, 2006.
17) Nimura A, Muneta T, Koga H, et al : Human synovial mesenchymal stem cells increase with human autologous serum ; A comparison to fetal bovine serum and to bone marrow cells. Arthritis Rheum **58** (2) : 501-510, 2008.
18) Koga H, Shimaya M, Muneta T, et al : Local adherent technique for transplanting mesenchymal stem cells as a potential treatment of cartilage defect. Arthritis Res Ther **10** (4) : R84, 2008.
19) Koga H, Muneta T, Ju YJ, et al : Synovial stem cells are regionally specified according to local microenvironments after implantation for cartilage regeneration. Stem Cells **25** (3) : 689-696, 2007.
20) Shimaya M, Muneta T, Ichinose S, et al : Magnesium enhances adherence and cartilage formation of synovial mesenchymal stem cells through integrins. Osteoarthritis Cartilage **18** (10) : 1300-1309, 2010.

Q 軟骨再生の概要と応用の可能性

軟骨は再生しないというのが長年の常識とされていたが，近年の再生医療の進歩により，軟骨再生が可能になりつつあると聞く．治療法の概要と適応について．また，今後の医療応用の可能性と展望（特に変形性膝関節症）はいかがか．

（埼玉県　M）

A 軟骨損傷に対する外科的治療として，骨髄刺激，骨軟骨柱移植，軟骨細胞移植等の方法が行われている．最近，骨髄液や滑膜等から採取した幹細胞を移植する方法が試みられている

（1）概　要

軟骨は細胞密度が低く，血行を欠くため，再生能力が低い組織である．軟骨下骨に達しない部分欠損は通常自然修復しない．

一方，軟骨下骨に達する全層欠損の修復は年齢，欠損の大きさや部位などに依存する．小さな欠損は硝子軟骨により修復されることもある．しかし，大きな欠損は修復されるとしても線維性組織や線維軟骨によって被覆される．この場合，正常軟骨より組織的，力学的に劣るため，結果として軟骨組織の変性，ひいては関節症性変化を引き起こす．軟骨損傷に対して，これまでにいくつかの外科的治療法が開発されている．

（2）治療法

①骨髄刺激法

マイクロフラクチャーやドリリングによる骨髄刺激法は軟骨下骨を外科的に穿孔し，骨髄からの出血を促し，軟骨前駆細胞の遊走や，損傷部位でのサイトカイン産生を期待するものである．手技が他よりも容易で特別な器具を必要とせず，低コストであることから，最も普及している方法である．しかし結果が安定せず，線維組織もしくは線維軟骨による修復となる．

②骨軟骨柱移植

骨軟骨柱移植（モザイクプラスティ）は，膝蓋大腿関節の大腿骨溝の端や大腿骨顆間の非荷重部から軟骨を骨とともに円柱状に採取し，軟骨欠損部位に1つ，あるいは複数個の骨軟骨柱をプレスフィットさせ移植するものである．硝子軟骨で修復される利点があるが，採取する正常骨軟骨柱の数に限界があり，手術侵襲が他のものと比較して大きい．

③自家培養軟骨細胞移植

自家培養軟骨細胞移植は，膝関節の非荷重部位より軟骨組織を採取し，体外で酵素処理後軟骨細胞を分離・増殖し，コラーゲンゲルに包埋した軟骨細胞を移植し，骨膜や人工素材シートで覆い周囲正常軟骨組織に縫合して固定するものである．国内では治験が終了した[1]．平成21年にJ-TEC社から製造販売承認申請が厚労省に提出されている．

（3）滑膜幹細胞移植による軟骨再生

骨髄液や滑膜などの間葉組織中には，よく増殖し，軟骨や骨に分化する能力のある間葉幹細胞が存在する．軟骨細胞は増殖能力が低く，さらに増殖させると脱分化して軟骨細胞の特徴が低下する．このため，細胞数を大量に確保することが難しい．しかし，間葉幹細胞では細胞数を十分確保できる利点がある[2]．筆者らは，滑膜由来の間葉幹細胞が自己血清でよく増殖すること[3]，細胞の浮遊液を軟骨欠損部に10分間静置することにより6割以

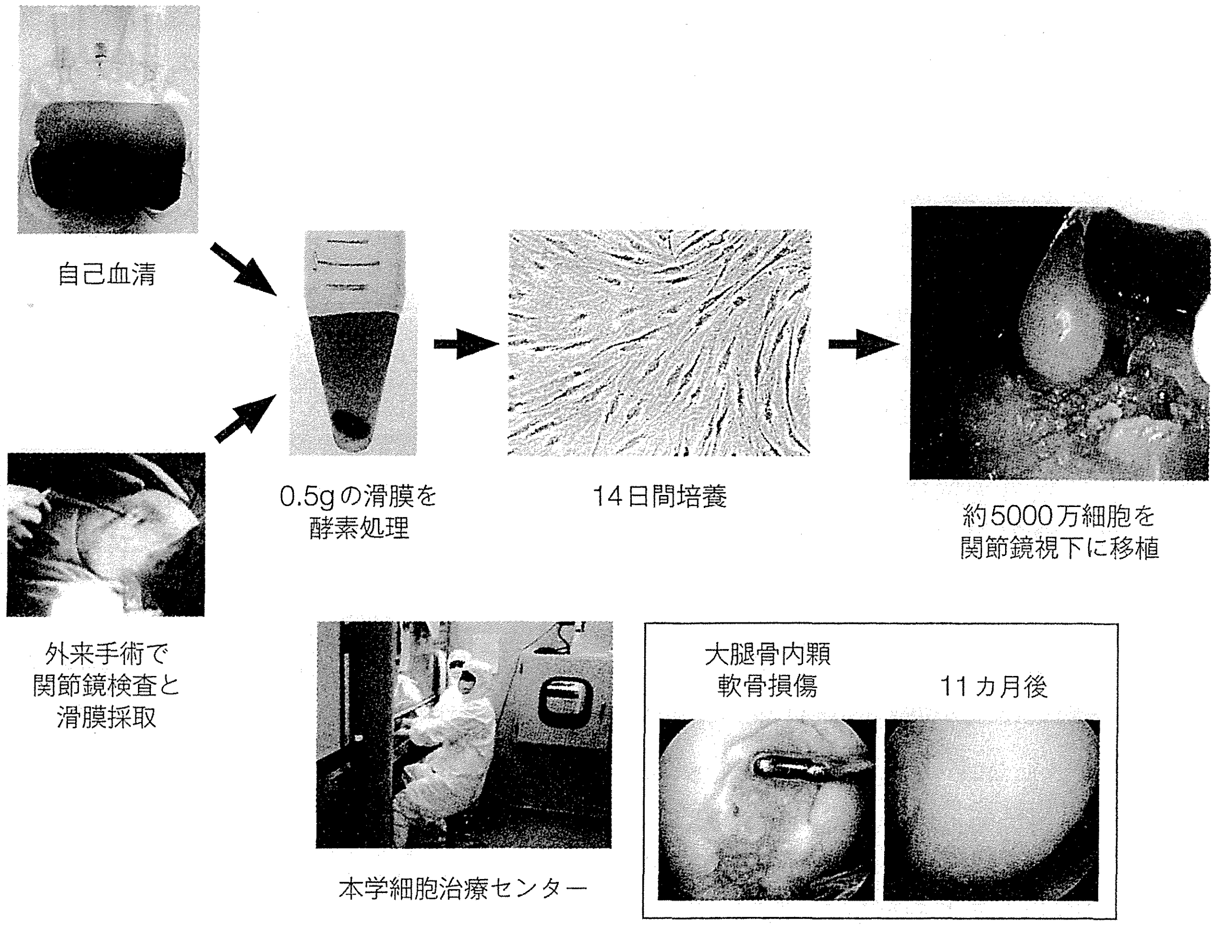

図1　軟骨欠損に対して滑膜幹細胞を関節鏡視下で移植する再生医療

上の細胞が軟骨欠損部に接着すること[4]，未分化な状態の細胞を軟骨欠損部に接着すると環境に応じて分化し，軟骨の基質を産生して軟骨欠損部が軟骨基質で覆われること[5]を基礎研究で明らかにした．

この成果に基づき，3年前から臨床研究を行っている．まず末梢血を採取し，自己血清を分離して用意する．外来手術で関節鏡検査と同時に滑膜を採取する．本学の手術室と同じフロアにある細胞治療センターで，滑膜を酵素処理後，10%自己血清を用いて滑膜間葉幹細胞を14日間培養する．平均0.5gの滑膜と70mLの自己血清から，14日間で平均5000万細胞を採取できる．この細胞の浮遊液を関節鏡視下で軟骨欠損部に10分間静置する．

後療法は，外固定をせず，2週後から部分荷重，6週後から全荷重を開始する．この方法は動物血清や人工素材を必要とせず，低侵襲で実施可能である利点がある．これまで重篤な副作用を認めていない．多数の例で軟骨欠損部の再生，症状の改善を認めている（図1）．

軟骨は再生しないというのが長年の常識となっていたが，近年の再生医療の進歩で，主に外傷性の軟骨損傷に対しては，低侵襲な方法で再生できるケースも出てきたと言える．

（4）変形性膝関節症に対する再生医療

高齢化社会において，変形性膝関節症に対する再生医療の開発が期待されている．変形性膝関節症に対して細胞移植を施行した再生

医療は，Wakitaniら[6]により報告されている．これは高位脛骨骨切術の際に，大腿骨内顆にコラーゲンゲルに包埋した骨髄間葉幹細胞を移植し，骨膜で被覆固定したものである．骨切術を行い細胞移植を施行しないコントロール群よりも，移植群は再鏡視及び生検所見が優れていた．ただし，臨床症状は変わらなかった．

この報告は変形性膝関節症の再生医療の難しさを示している．変形性膝関節症の患者の症状が，必ずしも軟骨を再生させることで解決しないことが，治療成績を短期間で評価する際の難しい点である．

(5) 今後の課題と展望

変形性膝関節症の病因や悪化因子は，常に複数あり，関節軟骨のみを一時的に再生できても，再度変性が進行するリスクを有する．アライメント不良例では骨切術が必要と考えられるが，その侵襲は大きい．また筆者らの臨床経験では，間葉幹細胞を軟骨障害部に移植すると，その細胞が軟骨組織に再生するかは，隣接する半月板の状態に影響を受ける．変形性膝関節症では半月板の変性・摩耗や逸脱を伴い，半月板に対する再生医療を含めた取り組みも必要となる[7]．

患者個々の変形性膝関節症の病態を考え，その病態に応じた複数の低侵襲な治療法を選択するのが，予防を含めた今後の目指すべき治療方法と考える．

▶文　献

1) Tohyama H, et al：J Orthop Sci 14：579, 2009.
2) Sekiya I, et al：Stem Cells 20：530, 2002.
3) Nimura A, et al：Arthritis Rheum 58：501, 2008.
4) Koga H, et al：Arthritis Res Ther 10：R84, 2008.
5) Koga H, et al：Stem Cells 25：689, 2007.
6) Wakitani S, et al：Osteoarthritis Cartilage 10：199, 2002.
7) Horie M, et al：Stem Cells 27：878, 2009.

▶回　答

東京医科歯科大学大学院医歯学総合研究科
軟骨再生学教授

関矢一郎

Free Radical Biology & Medicine 52 (2012) 607–615

Contents lists available at SciVerse ScienceDirect

Free Radical Biology & Medicine

journal homepage: www.elsevier.com/locate/freeradbiomed

Original Contribution

Lycopene inhibits *Helicobacter pylori*-induced ATM/ATR-dependent DNA damage response in gastric epithelial AGS cells

Sung Hee Jang [a], Joo Weon Lim [a], Tomohiro Morio [b,*], Hyeyoung Kim [a,**]

[a] Department of Food and Nutrition, Brain Korea 21 Project, College of Human Ecology, Yonsei University, Seoul 120-749, Korea
[b] Department of Pediatrics and Developmental Biology, Tokyo Medical and Dental University, Graduate School of Medical and Dental Sciences, Tokyo 113-8519, Japan

ARTICLE INFO

Article history:
Received 3 June 2011
Revised 7 November 2011
Accepted 10 November 2011
Available online 20 November 2011

Keywords:
Lycopene
Helicobacter pylori
DNA damage
Gastric epithelial AGS cells
Free radicals

ABSTRACT

Oxidative stress linked to DNA damage is involved in the pathogenesis of *Helicobacter pylori*-associated gastric diseases. The DNA damage response (DDR) coordinates cell-cycle transitions, DNA repair, and apoptosis through the activation of ataxia–telangiectasia-mutated (ATM) and ATM and Rad3-related (ATR) and their target proteins. However, neither *H. pylori*-induced DDR nor the effects of antioxidants on the DNA damage have been established. This study aimed to investigate the detailed process of *H. pylori*-induced DNA damage and to examine whether lycopene, a natural antioxidant, inhibits DNA damage and cellular response of gastric epithelial AGS cells infected with *H. pylori*. AGS cells were cultured with *H. pylori* in Korean isolates and treated with or without lycopene. Cell viability, DNA damage indices, levels of 8-OH-dG, and reactive oxygen species (ROS) as well as cell-cycle distributions were determined. The activation of ATM, ATR, Chk1, and Chk2; histone H2AX focus formation; activation and induction of p53; and levels of Bax and Bcl-2 and poly(ADP-ribose) polymerase-1 (PARP-1) were assessed. The results showed that *H. pylori* induced apoptosis in AGS cells with increased Bax and decreased Bcl-2 expression as well as PARP-1 cleavage. Culture with *H. pylori* led to increases in intracellular ROS, 8-OH-dG, double-strand DNA breaks (DSBs), and DNA fragmentation. *H. pylori* induced activation of the ATM/Chk2 and ATR/Chk1 pathways, phosphorylation of H2AX and p53, and a delay in the progression of the cells entering the S phase. Lycopene inhibited *H. pylori*-induced increases in ROS, apoptosis, alterations in cell-cycle distribution, DSBs, and ATM- and ATR-mediated DDR in AGS cells. In conclusion, lycopene may be beneficial for treatment of *H. pylori*-induced gastric diseases associated with oxidative DNA damage.

Helicobacter pylori is an important risk factor for chronic gastritis, peptic ulcer, and gastric carcinoma [1]. One of the potential toxic factors involving *H. pylori*-induced gastric injury is reactive oxygen species (ROS). ROS are released from activated neutrophils and regulate signal transduction cascades, acting as key regulatory switches in many cellular processes. Because *H. pylori* exhibits chemotactic activity for neutrophils [2], the initial pathological abnormality described in *H. pylori*-induced gastritis is the neutrophil infiltration of the gastric epithelium, a hallmark of active infection. Our previous studies have shown that *H. pylori* stimulated the production of ROS in gastric epithelial cells in the absence of inflammatory cells. This increase in ROS was determined by elevated levels of lipid peroxides, an index of oxidative membrane damage [3,4]. As a source of the infected cells, our recent study showed that *H. pylori* activates NADPH oxidase by inducing translocation of heat shock protein 90β from the cytosol to the membrane, leading to the activation of Rac1, a component of the NADPH oxidase complex [5], and increases the production of ROS in gastric epithelial cells [6]. *H. pylori* directly increased transcription levels of inflammatory cytokines by activating oxidant-sensitive transcription factors NF-κB and AP-1 [7] and induced apoptosis in gastric epithelial cells [8]. Antioxidants such as mannitol, dimethylthiourea, glutathione, and β-carotene effectively suppressed the induction of IL-8 and cyclooxygenase-2 by suppressing NF-κB and AP-1 in *H. pylori*-infected gastric epithelial cells [3,9,10]. Lycopene showed antioxidant activity and inhibited IL-6 expression by suppressing NF-κB activation in pancreatic acinar cells [11]. Inhibition of ROS production by lycopene prevented a decrease in DNA repair Ku proteins and apoptosis in pancreatic acinar cells [12]. We showed that *H. pylori*-induced activation of NF-κB mediated downregulation of Bcl-2 and induced apoptosis [13], whereas the antioxidant enzyme catalase inhibited NF-κB activation and apoptotic cell death in *H. pylori*-infected gastric epithelial cells [8]. Because ROS mediate NF-κB activation, lycopene may prevent oxidant-mediated apoptosis by inhibiting NF-κB activation and downregulation of Bcl-2 in *H. pylori*-infected gastric epithelial cells.

DNA damage caused by oxidative stress may be one important factor in the pathogenesis of *H. pylori*-associated gastric diseases [14]. Two of the major regulators of the DNA damage response (DDR) are

* Corresponding author. Fax: +81 3 5803 5245.
** Corresponding author. Fax: +82 2 364 5781.
E-mail addresses: tmorio.ped@tmd.ac.jp (T. Morio), kim626@yonsei.ac.kr (H. Kim).

0891-5849/$ - see front matter © 2011 Elsevier Inc. All rights reserved.
doi:10.1016/j.freeradbiomed.2011.11.010

phosphoinositide 3-kinase-related protein kinases, ataxia–telangiectasia mutated (ATM) and ataxia–telangiectasia and Rad3-related (ATR) [15]. ATM and ATR signals control cell-cycle transitions, DNA replication, DNA repair, and apoptosis and share many biochemical and functional similarities. The major functions of ATM and ATR in cell-cycle control are redundant; however, ATM and ATR respond to different types of DNA damage. ATM responds primarily to double-strand DNA breaks (DSBs), whereas ATR reacts to the structures that contain single-stranded DNA (ssDNA). This ssDNA is generated through many different types of DNA damage such as stalled replication forks and DSBs [16–18].

Formation of DSB ends leads not only to the recruitment of the meiotic recombination protein-11 (Mre11)–Rad50–Nijmegen breakage syndrome protein-1 (Nbs1) (MRN) complex but also to conversion of dimeric ATM into monomeric phosphorylated ATM. Activated ATM then phosphorylates the C-terminal tail of the histone variant H2AX to produce γ-H2AX, the initial signal for the subsequent accumulation of DDR proteins. Activated ATM also phosphorylates other downstream targets, including checkpoint kinase 2 (Chk2). ssDNA bound to replication protein A is recognized by ATR through interaction with ATR-interacting protein and leads to activation of ATR with topoisomerase-binding protein-1. The activated ATR phosphorylates a large list of substrates including checkpoint kinase 1 (Chk1) [19]. The induction of p53 in response to DNA damage is coordinated by ATM and ATR. Both kinases phosphorylate p53 at Ser15 and other sites; stabilization of p53 is also influenced by Chk2 and Chk1, which are phosphorylated by ATM and ATR, respectively [20]. These DDRs can be elicited by ROS and culminate in cell-cycle arrest, DNA repair, and, when unrepaired, apoptosis.

H. pylori-induced DNA damage leads to the activation of p53 and apoptosis in infected cells and tissues [21,22]. *H. pylori* not only inhibits cell-cycle progression at G1–S but also causes apoptosis by inducing the expression of cyclin D1 and p53 in gastric epithelial AGS cells [23,24]. *H. pylori* releases a factor that inhibits G1-to-S progression by affecting cyclin E/cyclin-dependent kinase 2 (Cdk2) kinase activity [25]. A recent study showed that *H. pylori* γ-glutamyl transpeptidase induces apoptosis and cell-cycle arrest at the G1–S phase transition and that this induction is also associated with downregulation of cyclin E, cyclin A, Cdk4, and Cdk6 and with upregulation of the Cdk inhibitors p27 and p21 in gastric epithelial AGS cells [26]. There have been reports on the direct effects of *H. pylori* on the inflammatory response, ROS production, cell-cycle progression, and apoptosis. However, a detailed analysis of the DDR elicited by *H. pylori* and the measures required to inhibit resulting DNA damage has not yet been explored.

Lycopene, a natural pigment synthesized by plants and microorganisms, has a high number of conjugated dienes, making it one of the most potent singlet oxygen quenchers among natural carotenoids [27]. Epidemiological studies have demonstrated that lycopene is associated with decreased risk of chronic diseases including cardiovascular diseases and cancers [28,29]. Lycopene has been shown to decrease oxidative DNA damage in lung fibroblasts [30], endothelial cells [31], and hepatocytes [32] caused by the redox cycling of catechol estrogens, H_2O_2, or γ-radiation. Lycopene also has antiproliferation and prodifferentiation activities in various types of cancer cells [33]. Therefore, lycopene has gained attention as a promising chemopreventive agent because of its antioxidant activity.

This study aimed to investigate *H. pylori*-induced DDR and the effect of lycopene on *H. pylori*-induced DNA damage in gastric epithelial AGS cells. We examined DNA damage indices (DNA fragmentation, DNA tail assessment, levels of 8-hydroxy-2′-deoxyguanosine (8-OH-dG)), levels of ROS, and alterations in the cell-cycle distribution. We also investigated the downstream events of *H. pylori*-induced activation of ATM and ATR, the expression of apoptosis-related proteins such as Bax and Bcl-2, and the cleavage of poly(ADP-ribose) polymerase-1 (PARP-1). We not only assessed the effect of lycopene on the amelioration of the reaction, but we also demonstrated that *H. pylori*-induced DDRs are caused by ROS.

Materials and methods

Bacterial strain

H. pylori in Korean isolates (HP99), the cagA^{+}, vacA s1bm2, iceA1 *H. pylori* strain [7], was inoculated onto chocolate agar plates (Becton–Dickinson Microbiology Systems, Cockeysville, MD, USA) at 37 °C under microaerophilic conditions using an anaerobic chamber (Becton–Dickinson Microbiology Systems).

Cell culture and H. pylori infection

Human gastric epithelial AGS cells (gastric adenocarcinoma, ATCC CRL 1739) were cultured in RPMI 1640 medium supplemented with 10% fetal bovine serum and penicillin/streptomycin. The cells were seeded and cultured overnight to reach 80% confluency. Before *H. pylori* infection, each well was washed once with 2 ml of fresh cell culture medium containing no antibiotics. Whole *H. pylori* was harvested from chocolate agar plates, suspended in antibiotic-free RPMI 1640 medium supplemented with 10% fetal bovine serum, and used to treat AGS cells. AGS cells were cultured in the presence of *H. pylori* at a 50:1 multiplicity of infection (m.o.i.). To investigate the effects of lycopene, the cells were treated with lycopene (Sigma, St. Louis, MO, USA) dissolved in tetrahydrofuran (final concentrations of 2 and 5 μM) for 1 h before *H. pylori* infection. The control group received tetrahydrofuran instead of lycopene. Because lycopene at 2 and 5 μM showed potent antioxidant activities in our previous studies [11,12], these concentrations were used in the present study to determine the effects of lycopene on *H. pylori*-induced DNA damage response in AGS cells.

Cell viability and DNA fragmentation

Viable cell numbers were determined using trypan blue exclusion test (0.2% trypan blue). DNA fragmentation was assessed according to the amount of oligonucleosome-bound DNA in the cell lysate using a Cell Death Detection ELISA^{plus} kit (Roche Molecular Biochemicals GmbH, Germany).

Determination of 8-OH-dG

Oxidative DNA damage was evaluated based on the generation of 8-OH-dG using a Biotrin OxyDNA assay kit (BD Biosciences, Dublin, Ireland). The formation of 8-OH-dG adducts in each sample was analyzed using flow cytometry (Beckman, Fullerton, CA, USA).

Neutral comet assay (single-cell gel electrophoresis)

Cells were suspended in 0.5% low-melting-point agarose and transferred onto a frosted glass microscope slide precoated with layer of 0.5% agarose. The slides were incubated in lysis solution (2.5 M NaCl, 100 mM Na_2 EDTA, 10 mM Trizma base, 1% *N*-lauroylsarcosine, NaOH to pH 10.0, and 1% v/v Triton X-100) at 4 °C for 1 h and electrophoresed at 25 V for 40 min. Comet tails were stained with SYBR green and analyzed by fluorescence microscope. In total, over 70 cells were analyzed per treatment using Scion Image (using scion_comet 1.3) with the comet assay for the comet tail moment.

Measurement of intracellular ROS

For the experiment on the time course of ROS production, the cells were cultured in the presence of *H. pylori* for 0, 15, 30, and 60 min. For the effects of lycopene, the cells were treated with lycopene for 1 h before *H. pylori* infection and cultured for 1 h. At each time period, the cells were loaded with 10 μM dichlorofluorescein diacetate (DCF-DA; Molecular Probes, Eugene, OR, USA) for 30 min, washed, and scraped off into 1 ml of PBS. The fluorescent dichlorofluorescein (DCF) was measured (excitation at 495 nm and emission at 535 nm) with a VICTOR2 multilabel counter (PerkinElmer Life and Analytical Sciences, Boston, MA, USA) or a laser scanning confocal microscope (Leica TCS-NT, Heidelberg, Germany) for the experiment with lycopene.

Cell-cycle analysis

The cells were trypsinized and washed twice with cold PBS. The pellet was treated with 1% (w/v) paraformaldehyde, followed by ice-cold 70% (v/v) ethanol for at least 12 h. After two washes with PBS, the cells were incubated with RNase (200 μg/ml final concentration), stained with propidium iodide (100 μg/ml final concentration) for 30 min, and analyzed using flow cytometry on a FACSCalibur system equipped with argon ion laser (Becton–Dickinson Immunocytometry System, San Jose, CA, USA). Percentages of the cells in each phase were calculated using the Cell Modfit software program (Becton–Dickinson).

Western blot analysis

Samples containing equal amounts of protein were separated by 12% SDS–PAGE and transferred onto nitrocellulose membranes. After being blocked in 3% nonfat dry milk for 2 h, the membrane was incubated with polyclonal antibodies for phosphospecific forms of ATM, ATR, Chk1 (phospho-S345 residue), Chk2 (phospho-T68 residue), p53 (phospho-S15 residue), and H2AX (γ-H2AX, phospho-S139 residue) (all from Cell Signaling Technology, Beverly, MA, USA). Some of the other polyclonal antibodies used were total forms of Chk1, Chk2, H2AX, PARP-1 (full-length PARP-1 (116 kDa) and large fragment of PARP-1 (89 kDa)) (all from Cell Signaling Technology) and ATR, ATM, p53, Bax, Bcl-2, or actin (all from Santa Cruz Biotechnology, Santa Cruz, CA, USA) in TBS-T (Tris-buffered saline containing 0.15% Tween 20) containing 3% nonfat dry milk at 4 °C overnight. Anti-Nbs1 and anti-Rad50 antibodies were obtained from Calbiochem (San Diego, CA, USA), and anti-Mre11 polyclonal antibody was from Novus Biologicals (Littleton, CO, USA). After being washed with TBS-T, the immunoreactive proteins were visualized using goat anti-mouse secondary antibodies conjugated to horseradish peroxidase, followed by enhanced chemiluminescence (Santa Cruz Biotechnology). Actin served as a loading control. Proteins (molecular mass) used in the study were Chk1 (56 kDa), Chk2 (66 kDa), ATR (250 kDa), ATM (370 kDa), p53 (53 kDa), Bax (23 kDa), Bcl-2 (26 kDa), PARP-1 (116 kDa), cleaved PARP-1 (89 kDa), H2AX (15 kDa), Nbs1 (95 kDa), Mre11 (80 kDa), and Rad50 (150 kDa). For the ratio of Bax/Bcl-2 as a parameter of apoptotic cell death, the protein bands of Bax and Bcl-2 were scanned using a Bio-Rad scanner (GS-700) driven by volume analysis software and quantified with Molecular Analysis software (version 4.1).

Immunofluorescence analysis for γ-H2AX

The cells were fixed with cold ethanol for 10 min and permeabilized in 0.1% Triton X-100/PBS for 15 min. The cells were blocked in PBS containing 5% goat serum and 1% bovine serum albumin and then incubated with polyclonal rabbit anti-γ-H2AX antibody for 1 h, followed by rhodamine-labeled mouse anti-rabbit IgG antibody (final concentration, 2 μg/ml) for 1 h. The cells were washed with PBS and stained with 5 μg/ml DAPI (4′,6′-diamidino-2-phenylindole) for 10 min. After being washed with PBS, the cells were mounted onto diazabicyclooctane glycerol (50%) and viewed by a confocal laser scanning microscope (LSM 510 META, Carl Zeiss, Germany).The captured images were analyzed for relative quantification of γ-H2AX using ImageJ software. The DAPI-stained nucleus of each cell was selected and used for relative quantification of γ-H2AX. All the foci were counted manually.

Statistical analysis

The statistical differences were determined using one-way ANOVA and Newman–Keuls test. All values are expressed as means ± SE of four different experiments. A value of $p<0.05$ was considered statistically significant.

Results

H. pylori induces cell death and DNA damage in AGS cells

During the 24-h culture, cell viability was slightly decreased in *H. pylori*-infected cells compared with the cells without infection (Fig. 1A). With this decrease in cell viability, *H. pylori* elicited an increase in nucleosome-bound DNA, an index of DNA fragmentation (Fig. 1B). We then monitored DSBs through a neutral comet assay. Although the comet formation was evident at 12 h, it continued to increase for at least 24 h (Fig. 1C). The cells infected with *H. pylori* showed a significant increment of comet cells with increased tail moments in a time-dependent manner. The results show a time-dependent increment of DNA damage in *H. pylori*-infected cells. An elevated 8-OH-dG level is an indicator of oxidative stress as well as DNA damage [34]. Uninfected AGS cells harbored relatively low levels of 8-OH-dG formation. In contrast, there were significant increases in

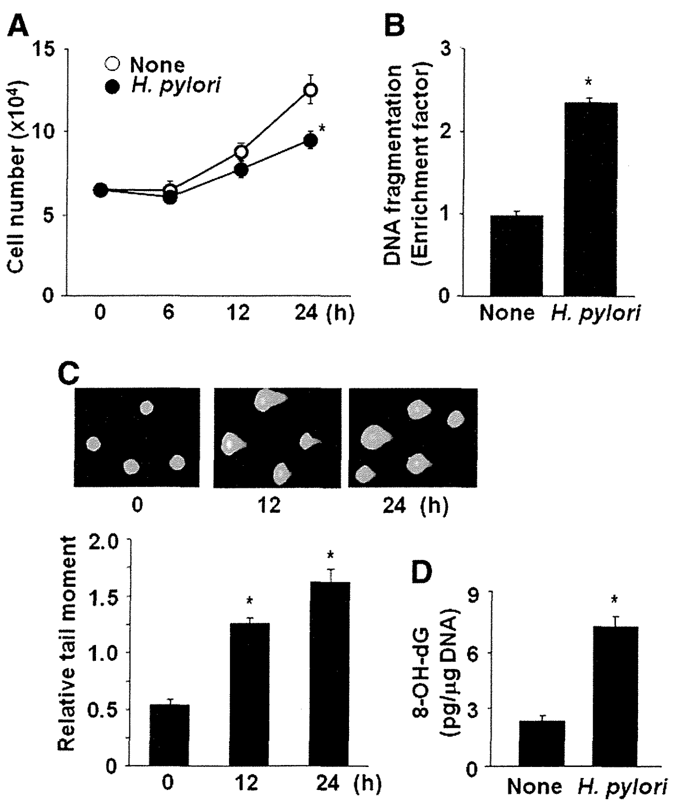

Fig. 1. *H. pylori* induces cell death and DNA damage in AGS cells. (A) Cell viability was determined using trypan blue exclusion test (0.2% trypan blue). (B) DNA fragmentation was assessed according to the amount of oligonucleosome-bound DNA in the cell lysate in 24-h culture. The relative increase in nucleosome-bound DNA, determined at 405 nm, was expressed as an enrichment factor. (C) DNA damage was examined using comet formation (top). Quantitative analysis of comet formation was assessed according to relative tail moment (bottom). (D) The levels of 8-OH-dG were analyzed fluorimetrically at 24 h culture. All values are expressed as means ± SE of four separate experiments. *$p<0.05$ for comparison to the corresponding "none" (the cells cultured in the absence of *H. pylori*) (A, B, D) or 0 h (C).

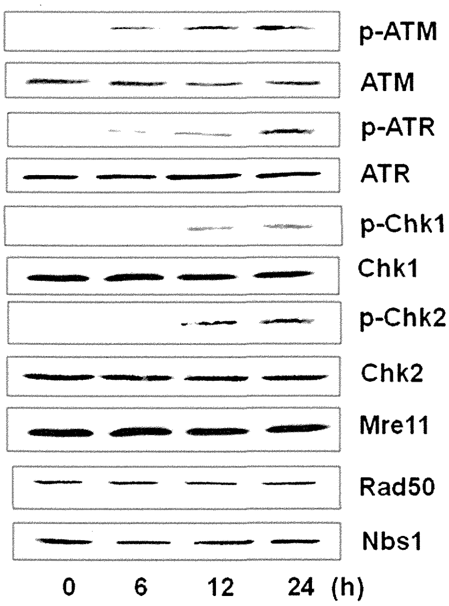

Fig. 2. *H. pylori* induces the phosphorylation of ATM, ATR, Chk1, and Chk2 in AGS cells. The levels of phosphospecific and total forms of ATM, ATR, Chk1, and Chk2 as well as total Mre11/Rad50/NBS1 were assessed using Western blot analysis, in which actin served as a loading control.

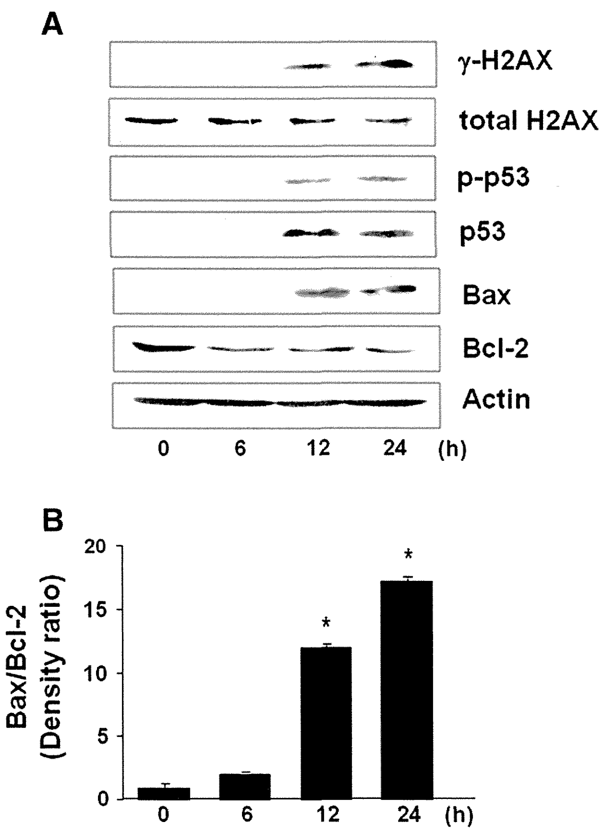

Fig. 3. *H. pylori* induces the phosphorylation of H2AX and p53 as well as alterations in the apoptotic indices of AGS cells. (A) The levels of phosphospecific and total forms of H2AX and p53 as well as apoptotic indices (Bax, Bcl-2) were determined via Western blot analysis in which actin served as a loading control. (B) The ratio of Bax/Bcl-2 was determined by the level of each protein that was scanned and expressed as density ratio. The ratio of Bax/Bcl-2 in the cells cultured in the presence of *H. pylori* at 0 h was considered as 1. All values are expressed as means ± SE of four separate experiments. *$p<0.05$ for comparison to the ratio at 0 h.

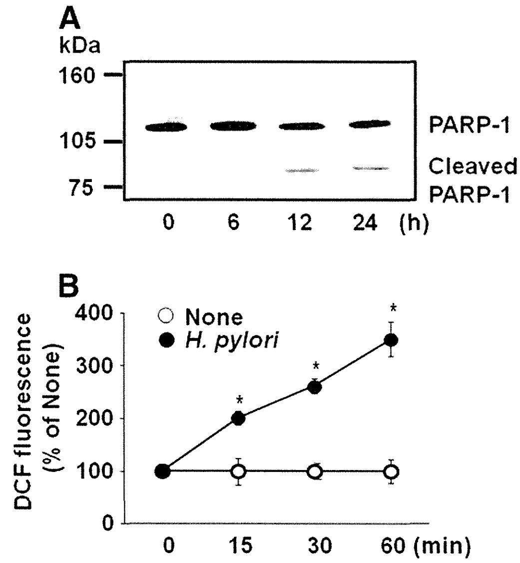

Fig. 4. *H. pylori* induces PARP-1 cleavage and an increase in ROS level of AGS cells. (A) The levels of PARP-1 (full-length PARP-1 (116 kDa) and large fragment of PARP-1 (89 kDa)) were determined via Western blot analysis. (B) ROS levels were determined by measuring the level of fluorescent DCF (excitation at 495 nm and emission at 535 nm). All values are expressed as means ± SE of four separate experiments. *$p<0.05$ for comparison to the corresponding "none" (the cells cultured in the absence of *H. pylori*).

8-OH-dG in *H. pylori*-infected AGS cells at 24 h (Fig. 1D). All of these DNA damage responses were elicited by a relatively low m.o.i. (50:1).

H. pylori induces the activation of ATM, ATR, Chk1, Chk2, H2AX, and p53

To investigate whether *H. pylori*-induced DNA damage is linked to the activation of ATM and ATR (Fig. 2), the levels of the phosphospecific and total forms of ATM and ATR as well as their target molecules such as Chk2, Chk1, and p53 were determined in *H. pylori*-infected AGS cells. The phosphorylation of ATM and ATR that was observed at 6 h increased through 24 h, whereas the total forms of ATM and ATR were not changed by *H. pylori* infection. *H. pylori* infection in AGS cells induced phosphorylation of Chk2 on T68 and Chk1 on residue S345 at 12 h, indicating the activation of ATM (Chk2) and ATR (Chk1) (Fig. 2). The total amounts of Chk2 and Chk1 as well as that of Mre11/Rad50/NBS1 were not changed by *H. pylori* infection. The phosphorylated form of H2AX (γ-H2AX) is essential to the efficient recognition and/or repair of DSBs. Phosphorylation of H2AX on S139

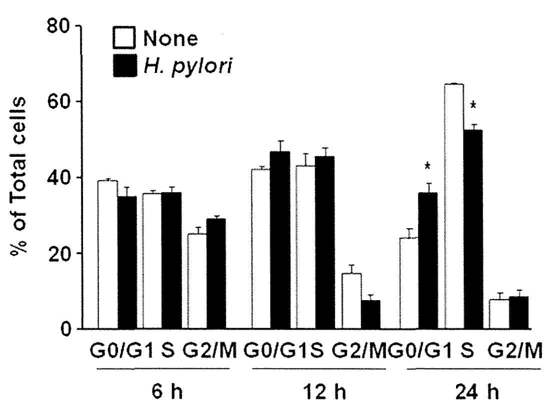

Fig. 5. *H. pylori* induces an alteration in cell-cycle distribution of AGS cells. After the cells were harvested, they were incubated with RNase and stained with propidium iodide. Flow cytometric analysis was performed to analyze the cell-cycle distribution. Percentages of the cells in each phase were calculated using the Cell Modfit software program. All values are expressed as means ± SE of four separate experiments. *$p<0.05$ for comparison to the corresponding "none" (the cells cultured in the absence of *H. pylori*).

was noted in AGS cells at 12 h, a trend that increased through 24 h (Fig. 3A). p53 is a target substrate of ATM, ATR, Chk2, and Chk1 after DDR. Phosphorylation of residue S15 of p53 was increased in *H. pylori*-infected cells (Fig. 3A) and was accompanied by the induction of p53 that is caused by stabilization of p53 protein. These results suggest that *H. pylori* induces DSBs at low m.o.i. and activates ATM and ATR DNA damage response pathways. These alterations may lead to the phosphorylation and stabilization of p53 for apoptotic cell death, alterations in cell-cycle distribution, or both.

H. pylori induces alterations in Bax and Bcl-2 as well as PARP-1 cleavage in AGS cells

p53 is known to mediate the downregulation of Bcl-2 as well as upregulation of Bax [35,36]. We next investigated the expression levels of the Bcl-2 family of apoptosis regulator proteins. As shown in Fig. 3, *H. pylori* induced an increase in Bax and a decrease in Bcl-2 (Fig. 3A) as well as an increase in the density ratio of Bax/Bcl-2 (Fig. 3B) in AGS cells. It is highly likely that the upregulation of p53 in AGS cells triggered by the DNA damage response to *H. pylori* led to the changes in the levels of Bax and Bcl-2, which then led to cellular apoptosis.

PARP-1 is involved in the DNA repair process and links DNA damage with apoptosis. Because PARP-1 is a substrate of caspase-3, PARP-1 cleavage reflects apoptotic cell death [37]. We previously showed that oxidative stress induced the activation of caspase-3 and nuclear loss of DNA repair Ku proteins in pancreatic acinar cells [38]. Therefore, ROS produced by *H. pylori* infection may activate caspase-3 and concurrently cleave PARP-1 in gastric epithelial cells. In Fig. 4A, the large fragment of PARP-1 was observed at 12 and 24 h in *H. pylori*-infected cells. The result demonstrates that PARP-1 cleavage may contribute to DNA damage and apoptosis in *H. pylori*-infected cells.

H. pylori induces increases in ROS levels in AGS cells

To determine the oxidative stress in AGS cells due to a low m.o.i. of *H. pylori*, intracellular levels of ROS were determined using DCF-DA via flow cytometry (Fig. 4B). Treatment with *H. pylori* resulted in an increase in the intracellular ROS level shown in AGS cells at 15-min culture. This increase in ROS continued for at least 60 min. These results combined with the data showing activation of the DNA damage response pathway suggest that ROS produced by *H. pylori* may mediate DNA damage and cell death in AGS cells.

H. pylori induces alterations in cell-cycle distribution of AGS cells

We then monitored whether *H. pylori* affected the cell-cycle progression in AGS cells. Flow cytometric analysis of the AGS cell distribution in the absence of *H. pylori* showed that 25, 66, and 9% of AGS cells were in the G0–G1, S, and G2–M phases at 24 h, respectively (Fig. 5). AGS cells infected with *H. pylori* showed an increase in the percentage of epithelial cells in G0–G1 from 25 to 37%, with a decrease in S phase from 66 to 52% at 24 h. After infection by *H. pylori*, AGS cells advanced quickly through the G0–G1 phase in 12 h, followed by a delay in the progression of the cells entering the S phase at 24 h. After the first 6 h, the distribution of the uninfected AGS cells showed that 39, 36, and 25% of the cells were in the G0–G1, S, and G2–M phases, respectively. These values were not significantly changed by *H. pylori* infection at 6 h culture. Lycopene itself had no effect on cell-cycle distribution of uninfected AGS cells (data not shown).

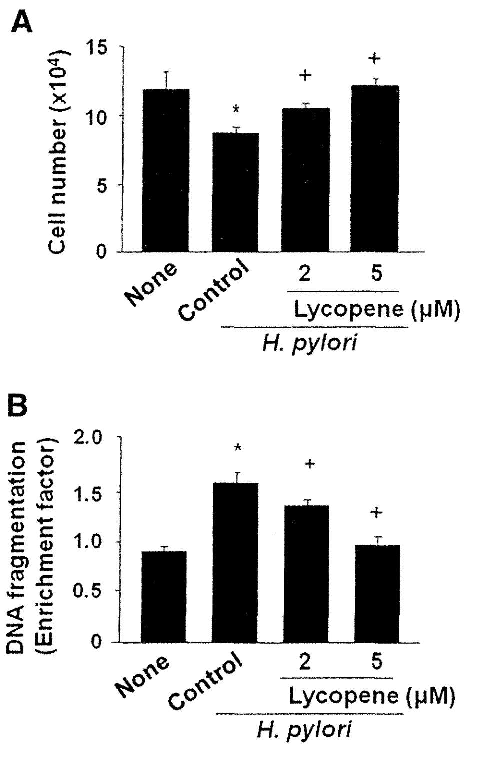

Fig. 6. Lycopene inhibits *H. pylori*-induced cell death and DNA fragmentation in AGS cells. (A) Cell viability was determined through a trypan blue exclusion test at 24 h culture. (B) DNA fragmentation was assessed according to the amount of oligonucleosome-bound DNA in the cell lysate at 24 h culture. All values are expressed as means ± SE of four separate experiments. *$p < 0.05$ for comparison to "none" (the cells cultured in the absence of *H. pylori*); $^{+}p < 0.05$ for comparison to control (the cells cultured in the presence of *H. pylori* without lycopene).

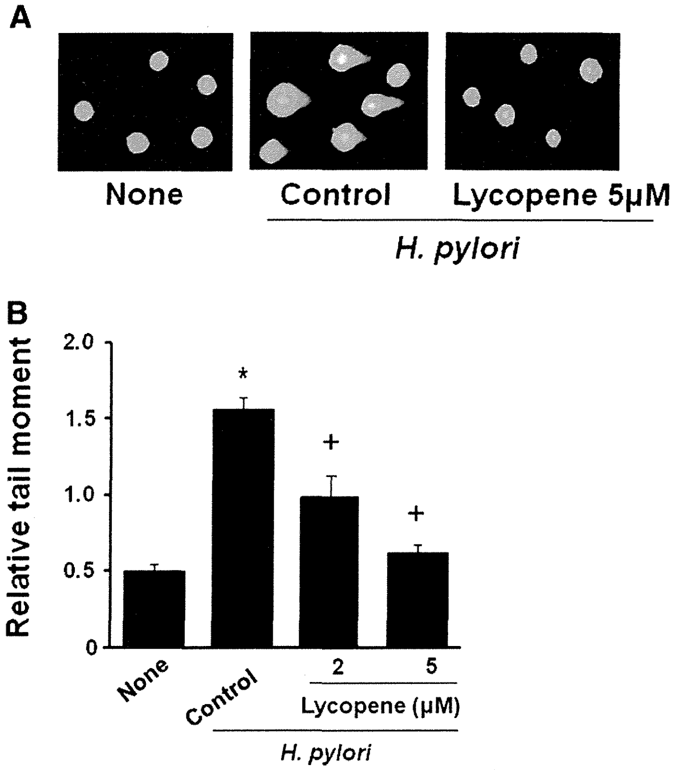

Fig. 7. Lycopene inhibits *H. pylori*-induced DNA damage in AGS cells, determined by comet assay. (A) DNA damage was examined using comet formation at 24 h culture. (B) Quantitative analysis of comet formation was assessed according to relative tail moment at 24 h culture. All values are expressed as means ± SE of four separate experiments. *$p < 0.05$ for comparison to "none" (the cells cultured in the absence of *H. pylori*); $^{+}p < 0.05$ for comparison to control (the cells cultured in the presence of *H. pylori* without lycopene).

Lycopene inhibits H. pylori-induced cell death, DNA damage, and γ-H2AX focus formation in AGS cells

To examine whether lycopene reverses *H. pylori*-induced DNA damage response and apoptosis, we treated *H. pylori*-infected cells with lycopene, a potent antioxidant, and monitored DNA damage responses and apoptosis. After 24 h culture, cell death and DNA fragmentation caused by *H. pylori* were inhibited by lycopene in a concentration-dependent manner (Figs. 6A and B). The addition of 5 μM lycopene almost completely inhibited *H. pylori*-induced DNA fragmentation in AGS cells. We then determined DSBs through a neutral comet assay. As shown in Fig. 7, treatment of *H. pylori* significantly increased comet formation (Fig. 7A) and tail moments (Fig. 7B) at 24 h, which was inhibited by lycopene treatment concentration dependently.

To further assess whether lycopene inhibits *H. pylori*-induced DNA damage, we examined the γ-H2AX focus formation, a commonly used in situ marker of DNA double-strand breaks, in *H. pylori*-infected cells treated with or without lycopene (Fig. 8). Immunofluorescence analysis for γ-H2AX shows that at 12 h culture, γ-H2AX focus formation was dramatically increased in *H. pylori*-infected cells. Lycopene decreased the percentage of cells exhibiting γ-H2AX foci in *H. pylori*-infected cells (Fig. 8A). The relative quantification of γ-H2AX was presented as average γ-H2AX foci per cell (Fig. 8B) and relative γ-H2AX intensity using ImageJ software (Fig. 8C). All three measures clearly demonstrate the inhibitory effect of lycopene on γ-H2AX focus formation of *H. pylori*-infected cells in a concentration-dependent manner.

Lycopene inhibits H. pylori-induced activation of ATM, ATR, Chk1, Chk2, H2AX, and p53 as well as alterations in apoptotic indices in AGS cells

The inhibitory effects of lycopene on *H. pylori*-induced phosphorylation of ATM and ATR were shown at 2 μM and were evident at 5 μM concentration of lycopene at 12 h (Fig. 9). Similarly, lycopene suppressed the phosphorylation of Chk1 on S345, Chk2 on T68, p53 on S15, and H2AX on S139, which was induced by *H. pylori* in AGS cells (Figs. 9 and 10A). The total amounts of ATM, ATR, Chk1, and Chk2 as well as the expression of the MRN complex were not changed by *H. pylori* infection with or without lycopene treatment. The induction of p53 by *H. pylori* was also suppressed by lycopene treatment.

Regarding apoptotic indices such as Bax and Bcl-2, lycopene inhibited the increase in Bax and the decrease in Bcl-2 as well as the increase in density of Bax/Bcl-2 in *H. pylori*-infected cells at 12 h (Figs. 10A and B). *H. pylori*-induced cleavage of PARP-1 was suppressed by lycopene dose dependently (Fig. 11A). Even though it is not clear whether the inhibitory effect of lycopene on the alterations in Bax and Bcl-2 are unequivocally related to the reduction of p53 induced by lycopene, the results show that *H. pylori*-induced DNA damage, the DNA damage

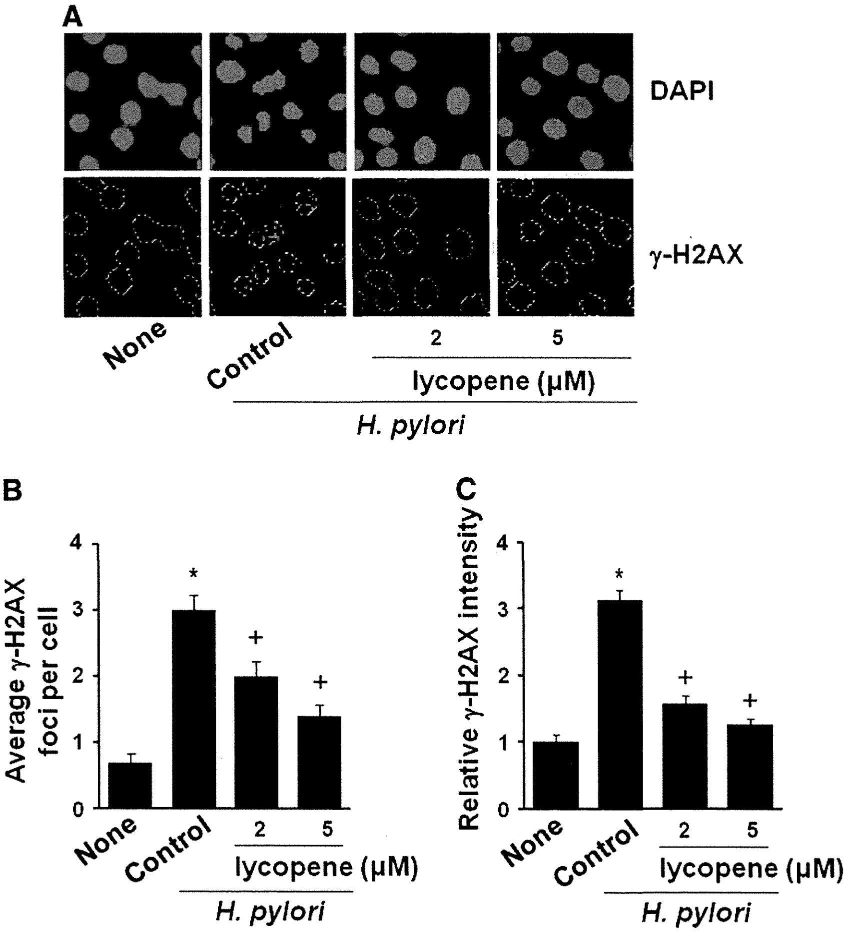

Fig. 8. Lycopene inhibits *H. pylori*-induced γ-H2AX focus formation in AGS cells. (A) At 12 h culture, the cells were stained with rabbit anti-γ-H2AX antibody and rhodamine-labeled mouse anti-rabbit IgG antibody. The cells were then stained with 5 μg/ml DAPI. The cells stained with rhodamine-labeled antibody and DAPI were examined with a laser scanning confocal microscopy. (B) Graph represents average number of γ-H2AX foci per cells. (C) Graph represents relative intensity of γ-H2AX as determined by ImageJ software. Results are expressed as means ± SE. *$p<0.05$ for comparison to "none" (the cells cultured in the absence of *H. pylori*); $^{+}p<0.05$ for comparison to *H. pylori* control (the cells cultured in the presence of *H. pylori* without lycopene).

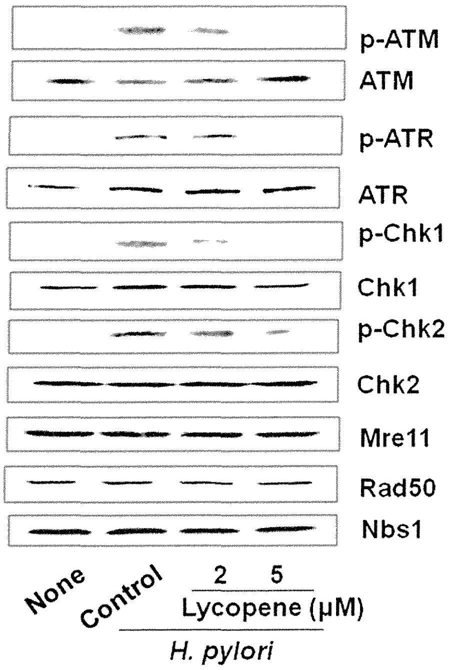

Fig. 9. Lycopene inhibits *H. pylori*-induced phosphorylation of ATM, ATR, Chk1, and Chk2 in AGS cells. At 12 h culture, the levels of phosphospecific and total forms of ATM, ATR, Chk1, and Chk2 as well as total Mre11/Rad50/Nbs1 of the cells were determined using Western blot analysis, in which actin served as a loading control.

response including the activation of ATM and ATR, and apoptosis are suppressed by lycopene treatment in AGS cells.

Lycopene inhibits the H. pylori-induced increase in ROS level and alterations in cell-cycle distribution in AGS cells

To further ensure that lycopene treatment affected ROS level in AGS cells, the intracellular levels of ROS were determined at 1 h using DCF-DA via confocal microscopy (Fig. 11B) and flow cytometry (Fig. 11C). Fig. 11 shows that the *H. pylori*-induced increase in ROS level was inhibited by lycopene in a concentration-dependent manner. Because lycopene, containing conjugated dienes, acts as a singlet oxygen quencher [27], antioxidant activity of lycopene may reduce the levels of ROS in *H. pylori*-infected AGS cells. In addition, lycopene may increase the activities and levels of antioxidant enzymes (SOD, catalase, glutathione peroxidase) in gastric epithelial cells as shown in a rat model of gastric cancer [39]. Treatment of AGS cells cultured in the presence of *H. pylori* with lycopene at a final concentration of 5 μM for 24 h decreased the proportion of cells in the G1 phase (from 37 to 26%), with a parallel increase in the proportion of cells in the S phase (from 52 to 65%) in *H. pylori*-infected AGS cells (Fig. 12), demonstrating that lycopene prevents *H. pylori*-induced delay in the progression of the cells entering the S phase at 24 h. G2–M phase was not changed in the cells, neither by *H. pylori* infection nor by lycopene treatment.

Discussion

This study demonstrates, for the first time, that *H. pylori* induces vigorous DDR that involves both ATM and ATR in a gastric epithelial cell line. Lycopene, a potent ROS-scavenging agent, rescued the *H. pylori*-infected cells from DNA damage and apoptosis.

Previously we found that *H. pylori* induced apoptosis and DNA damage in gastric epithelial cells. These inductions were suppressed by scavenging of hydrogen peroxide with catalase [8]. ROS production by *H. pylori* plays an important role in apoptosis and DNA damage processes in gastric epithelial cells [14]. Oxidative stress induces DNA damage that may well lead to apoptotic cell death, alterations in cell cycle distribution, or both. Although Chiou et al. reported that *H. pylori* inhibits G2–M to G1 progression in AGS cells [40], some studies have demonstrated that *H. pylori* and its γ-glutamyl transpeptidase inhibit cell-cycle procession at G1 and induce apoptosis [22–26]. *H. pylori*-induced p53 activation, which up-regulates the expression of p21, Bax, or both, has an important role in alterations in cell cycle distribution and apoptosis of AGS cells [22,23,41]. Recently, we found that downregulation of Bcl-2 is mediated by NF-κB activation in *H. pylori*-induced apoptosis of gastric epithelial cells [13]. In the present study, we demonstrated that *H. pylori* in Korean isolates (HP99) induced a delay in the progression of the cells entering the S phase, p53 activation, PARP-1 cleavage, upregulation of Bax, and a reciprocal decrease in Bcl-2 level in AGS cells. It is likely that p53 mediated the downregulation of Bcl-2 as well as the upregulation of Bax in *H. pylori*-infected cells, as has been shown in various cancer cells [35,36].

Some reports show that H_2O_2 and other peroxides induce ATM-dependent p53 phosphorylation in response to DNA damage, whereas others have shown that oxidative stress induces both ssDNA breaks (SSBs) and later DSBs. ATM is mainly activated by DSBs, whereas ATR

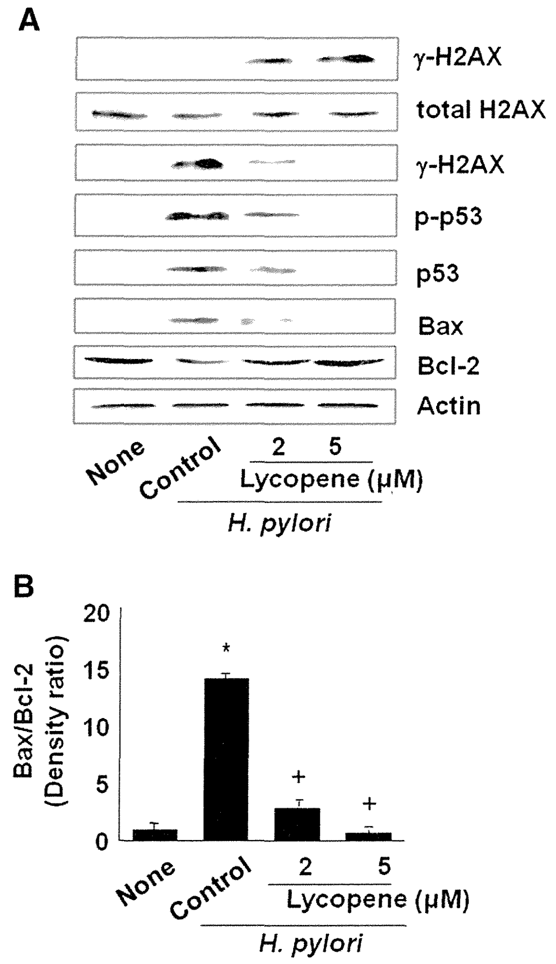

Fig. 10. Lycopene inhibits *H. pylori*-induced phosphorylation of H2AX and p53 as well as alterations in the apoptotic indices in AGS cells. (A) At 12 h culture, the levels of phosphospecific and total forms of p53 and γ-H2AX as well as apoptotic indices (Bax, Bcl-2) were assessed using Western blot analysis, in which actin served as a loading control. (B) The ratio of Bax/Bcl-2 was determined by the level of each protein, which was scanned and expressed as density ratio. The ratio of Bax/Bcl-2 in the cells cultured in the absence of *H. pylori* (none) was considered as 1. All values are expressed as means ± SE of four separate experiments. *$p<0.05$ for comparison to "none" (the cells cultured in the absence of *H. pylori*); $^{+}p<0.05$ for comparison to *H. pylori* control (the cells cultured in the presence of *H. pylori* without lycopene).

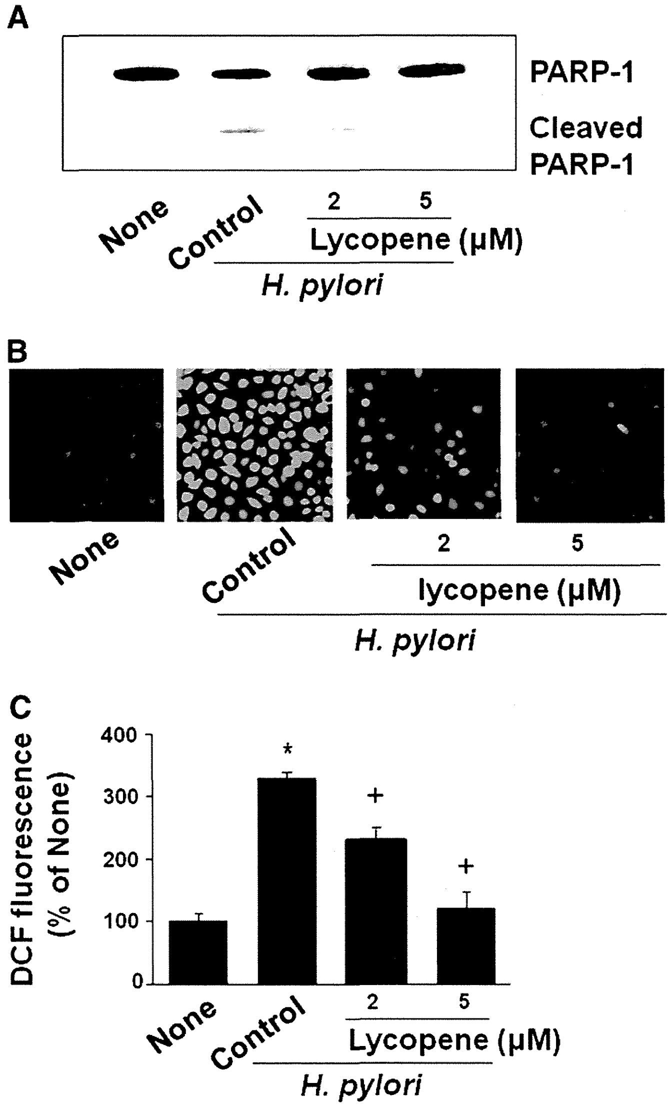

Fig. 11. Lycopene inhibits *H. pylori*-induced PARP-1 cleavage and the increase in ROS levels of AGS cells. (A) At 12 h culture, the levels PARP-1 (full-length PARP-1 (116 kDa) and large fragment of PARP-1 (89 kDa)) were determined via Western blot analysis. (B, C) At 60 min culture, ROS levels were determined using confocal microscopy (B) and by measuring the level of fluorescent dichlorofluorescein with excitation at 495 nm and emission at 535 nm (C). All values are expressed as means ± SE of four separate experiments. *$p<0.05$ for comparison to the corresponding "none" (the cells cultured in the absence of *H. pylori*); $^{+}p<0.05$ for comparison to *H. pylori* control (the cells cultured in the presence of *H. pylori* without lycopene).

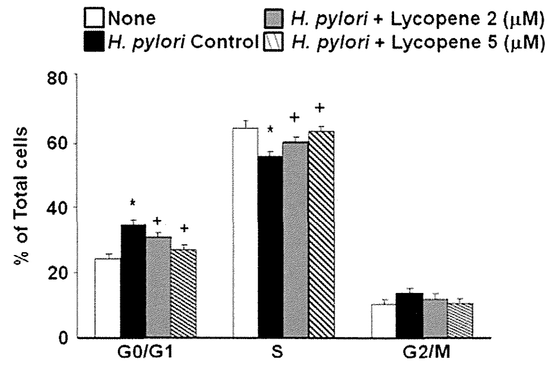

Fig. 12. Lycopene inhibits *H. pylori*-induced cell-cycle arrest in AGS cells. After the cells were harvested, they were incubated with RNase and stained with propidium iodide at 24 h culture. Flow cytometric analysis was performed to analyze the cell cycle distribution. Percentages of the cells in each phase were calculated using Cell Modfit software programs. All values are expressed as means ± SE of four separate experiments. *$p<0.05$ for comparison to the corresponding "none" (the cells cultured in the absence of *H. pylori*); $^{+}p<0.05$ for comparison to *H. pylori* control (the cells cultured in the presence of *H. pylori* without lycopene).

activation is triggered by SSBs [15–18]. Although ATM and ATR affect different DNA structures, both can be activated by DSBs because DSB end resection leads to a larger single-stranded region. In that sense, ATM and ATR are considered partners in the DSB response. Our data, including a neutral comet assay, demonstrated that DSBs are generated in *H. pylori* infection and that both ATM and ATR are activated by ROS-induced DNA damage in *H. pylori*-infected gastric epithelial cells.

H2AX, one of the key components of chromatin, becomes rapidly phosphorylated on the chromatin surrounding DSBs. Phosphorylated H2AX, γ-H2AX, forms "focuses" at DSBs, which are induced by ionizing radiation, meiosis, and replication [42]. ATM is the primary kinase that phosphorylates H2AX at DSB, although ATR and DNA-dependent protein kinase have also been implicated [43]. Our present study suggests that *H. pylori*-induced γ-H2AX focus formation in gastric epithelial cells is dependent on ATM and/or ATR.

ATM activates Chk2 to stabilize and activate p53, which then affects the G1 cell-cycle checkpoint in the immortalized cells [44]. Therefore, *H. pylori* may induce alterations in cell-cycle distribution through ATM/Chk2/p53 activation in gastric epithelial cells. Because *H. pylori* induces the activation of ATR and Chk1 in AGS cells in this study, we could not exclude the involvement of ATR in *H. pylori*-induced alterations in cell-cycle distribution and apoptotic cell death. Further study should be performed to determine the relationship among ATM, ATR, other DDR proteins, and cell-cycle control proteins in *H. pylori*-infected gastric epithelial cells.

In this study, we demonstrated that lycopene at 2 and 5 μM suppressed *H. pylori*-induced DNA damage, apoptosis, and increases in ROS levels in AGS cells. Palozza et al. demonstrated that lycopene at 0.5 and 2 μM prevents the G1 cell arrest induced by oxysterol [45]. Lycopene protected against H_2O_2-induced and aflatoxin-induced DNA damage and apoptosis in human endothelial cells [31] and HepG2 cells [46]. In humans, supplementation with tomato products or purified lycopene decreased oxidative DNA damage [47]. Furthermore, consumption of tomato and tomato juice induced lymphocyte DNA resistance to oxidative stress [48]. However, little is known about the detailed effects of lycopene on oxidative stress-induced apoptosis and DNA damage.

In this study, lycopene was shown to be effective in the prevention of cellular apoptosis, a delay in the progression of the cells entering the S phase, activation of p53, and activation of ATM/ATR in *H. pylori*-infected gastric epithelial cells. Therefore, lycopene may be beneficial for the prevention and/or treatment of *H. pylori*-associated gastric diseases. This benefit may occur by inhibiting oxidative DNA damage and the consequent DNA damage response such as alterations in cell-cycle distribution and thus apoptosis through suppression of ATM/Chk2/p53 activation as well as ATR/Chk1 activation. The mechanism of lycopene may be explained at least partially by its scavenging of ROS, which prevents oxidative DNA damage and DNA strand breaks in *H. pylori*-infected gastric epithelial cells.

In summary, we have shown that *H. pylori* induces a vigorous oxidative DNA damage response involving the ATM and ATR pathways in gastric epithelial cells. The infection results in a delay in the progression of the cells entering the S phase and apoptosis. Lycopene inhibited *H. pylori*-induced DNA damage and apoptosis probably by reducing the levels of ROS and thus suppressing the DNA damage response and alterations in cell-cycle distribution in gastric epithelial cells. Lycopene may be beneficial for the prevention and the treatment of *H. pylori*-induced gastric diseases linked to oxidative DNA damage.

Acknowledgments

This study was supported by the National Research Foundation of Korea (NRF) funded by the Ministry of Education, Science, and Technology (2010-0002916, 2011-0001177) and by a grant (Joint Research Project under the Korea-Japan Basic Scientific Cooperation Program) from the NRF (F01-2009-000-10101-0) (to H.K.) and from the JSPS (to T.M.).

References

[1] Marshall, B. J. *Helicobacter pylori*. *Am. J. Gastroenterol.* **89:**S116–S128; 1994.
[2] Craig, P. M.; Territo, M. C.; Karnes, W. E.; Walsh, J. H. *Helicobacter pylori* secretes a chemotactic factor for monocytes and neutrophils. *Gut* **33:**1020–1023; 1992.
[3] Kim, H.; Seo, J. Y.; Kim, K. H. Effects of mannitol and dimethylthiourea on *Helicobacter pylori*-induced IL-8 production in gastric epithelial cells. *Pharmacology* **59:**201–211; 1999.
[4] Kim, H.; Seo, J. Y.; Kim, K. H. Inhibition of lipid peroxidation, NF-kappaB activation and IL-8 production by rebamipide in *Helicobacter pylori*-stimulated gastric epithelial cells. *Dig. Dis. Sci.* **45:**621–628; 2000.
[5] Cha, B.; Lim, J. W.; Kim, K. H.; Kim, H. HSP90beta interacts with Rac1 to activate NADPH oxidase in *Helicobacter pylori*-infected gastric epithelial cells. *Int. J. Biochem. Cell Biol.* **42:**1455–1461; 2010.
[6] Cha, B.; Lim, J. W.; Kim, K. H.; Kim, H. 15-Deoxy-$\Delta^{12,14}$-prostaglandin J_2 suppresses RANTES expression by inhibiting NADPH oxidase activation in *Helicobacter pylori*-infected gastric epithelial cells. *J. Physiol. Pharmacol.* **62:**167–174; 2011.
[7] Seo, J. H.; Lim, J. W.; Kim, H.; Kim, K. H. *Helicobacter pylori* in a Korean isolate activates mitogen-activated protein kinases, AP-1, and NF-kappaB and induces chemokine expression in gastric epithelial AGS cells. *Lab. Invest.* **84:**49–62; 2004.
[8] Lim, J. W.; Kim, H.; Kim, K. H. NF-κB, inducible nitric oxide synthase and apoptosis by *Helicobacter pylori* infection. *Free Radic. Biol. Med.* **31:**355–366; 2001.
[9] Seo, J. Y.; Kim, H.; Kim, K. H. Transcriptional regulation by thiol compounds in *Helicobacter pylori*-induced interleukin-8 production in human gastric epithelial cells. *Ann. N. Y. Acad. Sci.* **973:**541–545; 2002.
[10] Jang, S. H.; Lim, J. W.; Kim, H. Beta-carotene inhibits *Helicobacter pylori*-induced expression of inducible nitric oxide synthase and cyclooxygenase-2 in human gastric epithelial AGS cells. *J. Physiol. Pharmacol.* **60** (Suppl. 7):131–137; 2009.
[11] Kang, M.; Park, K. S.; Seo, J. Y. Lycopene inhibits IL-6 expression in cerulein-stimulated pancreatic acinar cells. *Genes Nutr.* **6:**117–123; 2011.
[12] Seo, J. Y.; Masamune, A.; Shimosegawa, T.; Kim, H. Protective effect of lycopene on oxidative stress-induced cell death of pancreatic acinar cells. *Ann. N. Y. Acad. Sci.* **1171:** 570–575; 2009.
[13] Chu, S. H.; Lim, J. W.; Kim, D. G.; Lee, E. S.; Kim, K. H.; Kim, H. Down-regulation of Bcl-2 is mediated by NF-κB activation in *Helicobacter pylori*-induced apoptosis of gastric epithelial cells. *Scand. J. Gastroenterol.* **46:**148–155; 2011.
[14] Papa, A.; Danese, S.; Sgambato, A.; Ardito, R.; Zannoni, G.; Rinelli, A.; Vecchio, F. M.; Gentiloni-Silveri, N.; Cittadini, A.; Gasbarrini, G.; Gasbarrini, A. Role of *Helicobacter pylori* CagA$^+$ infection in determining oxidative DNA damage in gastric mucosa. *Scand. J. Gastroenterol.* **37:**409–413; 2002.
[15] Yang, J.; Xu, Z. P.; Huang, Y.; Hamrick, H. E.; Duerksen-Hughes, P. J.; Yu, Y. N. ATM and ATR: sensing DNA damage. *World J. Gastroenterol.* **10:**155–160; 2004.
[16] Cann, K. L.; Hicks, G. G. Regulation of the cellular DNA double-strand break response. *Biochem. Cell Biol.* **85:**663–674; 2007.
[17] Abraham, R. T. Cell cycle checkpoint signaling through the ATM and ATR kinases. *Genes Dev.* **15:**2177–2196; 2001.
[18] Zou, L.; Elledge, S. J. Sensing DNA damage through ATRIP recognition of RPA-ssDNA complexes. *Science* **300:**1542–1548; 2003.
[19] Cimprich, K. A.; Cortez, D. ATR: an essential regulator of genome integrity. *Nat. Rev. Mol. Cell Biol.* **9:**616–627; 2008.
[20] Barzilai, A.; Yamamoto, K. DNA damage responses to oxidative stress. *DNA Repair* **3:**1109–1115; 2004.
[21] Petersson, F.; Borch, K.; Franzen, L. E. Gastric epithelial proliferation and p53 and p21 expression in a general population sample: relations to age, sex, and mucosal changes associated with *H. pylori* infection. *Dig. Dis. Sci.* **47:**1558–1566; 2002.
[22] Wei, J.; Nagy, T. A.; Vilgelm, A.; Zaika, E.; Ogden, S. R.; Romero-Gallo, J.; Piazuelo, M. B.; Correa, P.; Washington, M. K.; El-Rifai, W.; Peek, R. M.; Zaika, A. Regulation of p53 tumor suppressor by *Helicobacter pylori* in gastric epithelial cells. *Gastroenterology* **139:**1333–1343; 2010.
[23] Gao, W.; Hu, F. L.; Lü, Y. Y. *Helicobacter pylori* inhibits cell growth and induces G1/S arrest in AGS gastric epithelial cells. *Zhonghua Yi Xue Za Zhi* **83:**731–735; 2003.
[24] Shirin, H.; Weinstein, I. B.; Moss, S. F. Effect of H. pylori infection of gastric epithelial cells on cell cycle control. *Front. Biosci.* **6:**E104–E118; 2001.
[25] Sommi, P.; Svio, M.; Stivala, L. A.; Scotti, C.; Mignosi, P.; Prosperi, E.; Vannini, V.; Solcia, E. *Helicobacter pylori* releases a factor(s) inhibiting cell cycle progression of human gastric cell lines by affecting cyclin E/cdk2 kinase activity and Rb protein phosphorylation through enhanced p27(KIP1) protein expression. *Exp. Cell Res.* **281:**128–139; 2002.
[26] Kim, K. M.; Lee, S. G.; Kim, J. M.; Kim, D. S.; Song, J. Y.; Kang, H. L.; Lee, W. K.; Cho, M. J.; Rhee, K. H.; Youn, H. S.; Baik, S. C. *Helicobacter pylori* gamma-glutamyltranspeptidase induces cell cycle arrest at the G1-S phase transition. *J. Microbiol.* **48:**372–377; 2010.
[27] Di Mascio, P.; Kaiser, S.; Sies, H. Lycopene as the most efficient biological carotenoid singlet oxygen quencher. *Arch. Biochem. Biophys.* **274:**532–538; 1989.
[28] Bhuvaneswari, V.; Nagini, S. Lycopene: a review of its potential as an anticancer agent. *Curr. Med. Chem. Anticancer Agents* **5:**627–635; 2005.
[29] Rao, A. V. Lycopene, tomatoes, and the prevention of coronary heart disease. *Exp. Biol. Med. (Maywood)* **227:**908–913; 2002.
[30] Muzandu, K.; El Bohi, K.; Shaban, Z.; Ishizuka, M.; Kazusaka, A.; Fujika, S. Lycopene and beta-carotene ameliorate catechol estrogen-mediated DNA damage. *Jpn. J. Vet. Res.* **52:**173–184; 2005.
[31] Tang, X.; Yang, X.; Peng, Y.; Lin, J. Protective effects of lycopene against H_2O_2-induced oxidative injury and apoptosis in human endothelial cells. *Cardiovasc. Drugs Ther.* **23:**439–448; 2009.
[32] Srinivasan, M.; Sudheer, A. R.; Pillai, K. R.; Kumar, P. R.; Sudhakaran, P. R.; Menon, V. P. Lycopene as a natural protector against γ-radiation induced DNA damage, lipid peroxidation and antioxidant status in primary culture of isolated rat hepatocytes in vitro. *Biochim. Biophys. Acta* **1770:**659–665; 2007.
[33] Levy, J.; Bosin, E.; Feldman, B.; Giat, Y.; Miinster, A.; Danilenko, M.; Sharoni, Y. Lycopene is a more potent inhibitor of human cancer cell proliferation than either alpha-carotene or beta-carotene. *Nutr. Cancer* **24:**257r. C; 1995.
[34] Tabak, O.; Gelisgen, R.; Erman, H.; Erdenen, F.; Muderrisoglu, C.; Aral, H.; Uzun, H. Oxidative lipid, protein, and DNA damage as oxidative stress markers in vascular complications of diabetes mellitus. *Clin. Invest. Med.* **34:**E163–E171; 2011.
[35] Miyashita, T.; Harigai, M.; Hanada, M.; Reed, J. C. Identification of a p53-dependent negative response element in the bcl-2 gene. *Cancer Res.* **54:**3131–3135; 1994.
[36] Zhang, N.; Kong, X.; Yan, S.; Yuan, C.; Yang, Q. Huaier aqueous extract inhibits proliferation of breast cancer cells by inducing apoptosis. *Cancer Sci.* **101:**2375–2383; 2010.
[37] Decker, P.; Muller, S. Modulating poly (ADP-ribose) polymerase activity: potential for the prevention and therapy of pathogenic situations involving DNA damage and oxidative stress. *Curr. Pharm. Biotechnol.* **3:**275–283; 2002.
[38] Song, J. Y.; Lim, J. W.; Kim, H.; Morio, T.; Kim, K. H. Oxidative stress induces nuclear loss of DNA repair proteins Ku70 and Ku80 and apoptosis in pancreatic acinar AR42J cells. *J. Biol. Chem.* **278:**36676–36687; 2003.
[39] Luo, C.; Wu, X. G. Lycopene enhances antioxidant enzyme activities and immunity function in N-methyl-N′-nitro-N-nitrosoguanidine-induced gastric cancer rats. *Int. J. Mol. Sci.* **12:**3340–3351; 2011.
[40] Chiou, C. C.; Chan, C. C.; Kuo, Y. P.; Chan, E. C. *Helicobacter pylori* inhibits activity of cdc2 kinase and delays G2/M to G1 progression in gastric adenocarcinoma cell line. *Scand. J. Gastroenterol.* **38:**147–152; 2003.
[41] Ahmed, A.; Smoot, D.; Littleton, G.; Tackey, R.; Walters, C. S.; Kashanchi, F.; Allen, C. R.; Ashktorab, H. *Helicobacter pylori* inhibits gastric cell cycle progression. *Microbes Infect.* **2:**1159–1169; 2000.
[42] Rogakou, E. P.; Boon, C.; Redon, C.; Bonner, W. M. Megabase chromatin domains involved in DNA double-strand breaks in vivo. *J. Cell Biol.* **146:**905–916; 1999.
[43] Burma, S.; Chen, B. P.; Murphy, M.; Kurimasa, A.; Chen, D. J. ATM phosphorylates histone H2AX in response to DNA double-strand breaks. *J. Biol. Chem.* **276:** 42462–42467; 2001.
[44] Chehab, N. H.; Malikzay, A.; Appel, M.; Halazonetis, T. D. Chk2/hCds1 functions as a DNA damage checkpoint in G(1) by stabilizing p53. *Genes Dev.* **14:**278–288; 2000.
[45] Palozza, P.; Simone, R.; Catalano, A.; Boninsegna, A.; Böhm, V.; Fröhlich, K.; Mele, M. C.; Monego, G.; Ranelletti, F. O. Lycopene prevents 7-ketocholesterol-induced oxidative stress, cell cycle arrest and apoptosis in human macrophages. *J. Nutr. Biochem.* **21:**34–46; 2010.
[46] Reddy, L.; Odhav, B.; Bhoola, K. Aflatoxin B1-induced toxicity in HepG2 cells inhibited by carotenoids: morphology, apoptosis and DNA damage. *Biol. Chem.* **387:**87–93; 2006.
[47] Porrini, M.; Riso, P. Lymphocyte lycopene concentration and DNA protection from oxidative damage is increased in women after a short period of tomato consumption. *J. Nutr.* **130:**189–192; 2000.
[48] Rehman, A.; Bourne, L. C.; Halliwell, B.; Rice-Evans, C. A. Tomato consumption modulates oxidative DNA damage in humans. *Biochem. Biophys. Res. Commun.* **262:**828–831; 1999.

RESEARCH ARTICLE

Human Mutation
OFFICIAL JOURNAL
HGVS
HUMAN GENOME VARIATION SOCIETY
www.hgvs.org

Functional Characterization and Targeted Correction of ATM Mutations Identified in Japanese Patients with Ataxia-Telangiectasia

Kotoka Nakamura,[1] Liutao Du,[1] Rashmi Tunuguntla,[1] Francesca Fike,[1] Simona Cavalieri,[2] Tomohiro Morio,[3] Shuki Mizutani,[3] Alfredo Brusco,[2] and Richard A. Gatti[1,4]*

[1]*Department of Pathology and Laboratory Medicine, UCLA School of Medicine, Los Angeles, California;* [2]*Department of Genetics, Biology and Biochemistry, University of Torino, Medical Genetics Unit, S. Giovanni Battista Hospital, Torino, Italy;* [3]*Department of Pediatrics and Developmental Biology, Tokyo Medical and Dental University Graduate School of Medicine, Tokyo, Japan;* [4]*Department of Human Genetics, UCLA School of Medicine, Los Angeles, California*

Communicated by Michel Goossens

Received 14 June 2011; accepted revised manuscript 15 September 2011.
Published online 17 October 2011 in Wiley Online Library (www.wiley.com/humanmutation).DOI: 10.1002/humu.21632

ABSTRACT: A recent challenge for investigators studying the progressive neurological disease ataxia-telangiectasia (A-T) is to identify mutations whose effects might be alleviated by mutation-targeted therapies. We studied ATM mutations in eight families of Japanese A-T patients (JPAT) and were able to identify all 16 mutations. The probands were compound heterozygotes in seven families, and one (JPAT2) was homozygous for a frameshift mutation. All mutations—four frameshift, two nonsense, four large genomic deletions, and six affecting splicing—were novel except for c.748C>T found in family JPAT6 and c.2639-384A>G found in family JPAT11/12. Using an established lymphoblastoid cell line (LCL) of patient JPAT11, ATM protein was restored to levels approaching wild type by exposure to an antisense morpholino oligonucleotide designed to correct a pseudoexon splicing mutation. In addition, in an LCL from patient JPAT8/9, a heterozygous carrier of a nonsense mutation, ATM levels could also be partially restored by exposure to readthrough compounds (RTCs): an aminoglycoside, G418, and a novel small molecule identified in our laboratory, RTC13. Taken together, our results suggest that screening and functional characterization of the various sorts of mutations affecting the *ATM* gene can lead to better identification of A-T patients who are most likely to benefit from rapidly developing mutation-targeted therapeutic technologies.

Hum Mutat 33:198–208, 2012.

KEY WORDS: ataxia-telangiectasia; ATM; large genomic deletions; functional analysis of DNA variants; mutation-targeted therapy; Japanese ATM mutation

Additional Supporting Information may be found in the online version of this article.

*Correspondence to: Richard A. Gatti, Department of Pathology and Laboratory Medicine, UCLA School of Medicine, 675 Charles E. Young Drive South, Los Angeles, CA 90095-1732. E-mail: rgatti@mednet.ucla.edu

Contract grant sponsors: National Institutes of Health (1R01NS052528); A-T Ease Foundation; A-T Medical Research Foundation.

Introduction

Ataxia-telangiectasia (A-T; MIM# 208900) is an autosomal recessive neurodegenerative disorder characterized by progressive cerebellar degeneration, ocular apraxia and telangiectasia, increased cancer risk, immunodeficiency, sensitivity to ionizing radiation (IR), chromosomal instability, and cell cycle abnormalities [Boder and Sedgwick, 1958; Gatti, 2001]. A-T is caused by mutations in the *ATM* gene (MIM# 607585) that usually encodes a 13 kb transcript that produces a 370 kDa protein [Gatti et al., 1988; Lange et al., 1995; Savitsky et al., 1995]. Intranuclear ATM protein is low or absent in most A-T patients, despite the presence of relatively normal levels of *ATM* transcripts. ATM is activated by autophosphorylation after binding with the MRN (Mre11-Rad50-Nbs) complex at sites of DNA double strand breaks [Bakkenist and Kastan, 2003; Kozlov et al., 2006], and subsequently phosphorylates hundreds of downstream target proteins involved in cell cycle checkpoints, DNA repair, and apoptosis [Bolderson et al., 2009; Matsuoka et al., 2007; Shiloh 2006]. ATM also appears to play a critical role in resolving chronic inflammation [Westbrook and Schiestl, 2010].

A-T patients are usually compound heterozygotes, carrying two distinct mutations. Mutations occur throughout the entire gene without hot spots. Founder effects are commonly observed in many ethnic isolates [Birrell et al., 2005; Campbell et al., 2003; Cavalieri et al., 2006; Gilad et al., 1996a; Laake et al., 1998; McConville et al., 1996; Mitui et al., 2003, 2005; Telatar et al., 1998a, b] wherein patients often carry mutations in a homozygous state. We have previously shown [Du et al., 2007, 2009, 2011; Lai et al., 2004] that accurately analyzing the functional consequences of mutations in individual A-T patients enables the grouping of patients into "mutation categories" that are most likely to be corrected by future customized mutation-targeted therapies.

The aims of the present study were to: (1) characterize the *ATM* mutations in Japanese A-T (JPAT) families; and (2) identify which JPAT patients might be candidates for personalized mutation-targeted therapy. We report that three of eight JPAT families examined are potential candidates for mutation-targeted therapy based on partial restoration of functional ATM protein production.

Materials and Methods

Cell Lines

Lymphoblastoid cell lines (LCLs) [Svedmyr et al., 1975] or activated T-cells [Minegishi et al., 2006] were established from affected members of eight Japanese A-T families, including three sibling pairs (JPAT4/5, 8/9, and 11/12). The families came from different geographical regions. Clinical descriptions of patients from these families have been reported previously [Morio et al., 2009].

Short Tandem Repeat (STR) Haplotype Analysis

Standardized STR (short tandem repeat/microsatellite) genotyping for the *ATM* gene region was performed as previously described [Mitui et al., 2003]. Briefly, we used four fluorescently labeled microsatellite markers located within a 1.4 cM region of chromosome 11q22-q23: D11S1819, NS22, D11S2179, and D11S1818. Markers NS22 and D11S2179 are located within the *ATM* gene, in introns 45 and 62, respectively [Udar et al., 1999; Vanagaite et al., 1995]. Allelic sizes were detected with an ABI 3730 DNA analyzer (Applied Biosystems Inc, Carlsbad, CA) and standardized to a reference sample (CEPH 1347-02).

Identification of Mutations

Total RNA was isolated from patient-derived T-cell lines using RNeasy (QIAGEN, Valencia, CA), and cDNA was synthesized using random primers and the Superscript III reverse transcriptase (Invitrogen, Carlsbad, CA). The entire *ATM* coding region was divided into eight overlapping fragments (Regions 1–8) ranging from 1,500 to 1,800 bps [Du et al., 2008]. These regions were PCR amplified and then sequenced using 19 different primers. Mutations on the cDNA level were confirmed in genomic DNA (gDNA) by sequencing relevant exon and intron boundaries. Mutation analysis is based on the same ATM reference sequence used for ATM mutations in the Leiden Open Variation Database (www.LOVD.nl/ATM; NCBI reference sequence:NM_000051.3).

Maximum Entropy Scores and Search for Exonic Splicing Enhancers (ESEs)

The strength of the 5′ and 3′ splice sites (ss) was determined by calculating and comparing the wild-type and mutant 5′ and 3′ ss using the Maximum Entropy software available at http://genes.mit.edu/burgelab/maxent/Xmaxentscan_scoreseq.html [Eng et al., 2004; Mitui et al., 2009; Yeo and Burge, 2004]. We scanned for putative binding motifs for serine/arginine-rich (SR) proteins using the ESEfinder software available at http://rulai.cshl.edu/tools/ESE [Cartegni et al., 2003; Smith et al., 2006].

Long-Range PCR and Breakpoint Regions for Genomic Deletions

To amplify large gDNA fragments, 500 ng of gDNA was used as template, followed by 35 cycles of 95C for 1 min, 68°C for 10 min, and extension at 72°C for 15 min using EX Taq polymerase according to the manufacturer's protocol (Takara Bio Inc, Shiga, Japan). Fragments containing large genomic deletions (LGDs) were isolated from agarose gels and sequenced to determine the breakpoints.

Multiplex Ligation-dependent Probe Amplification (MLPA)

A total of 100 ng of gDNA was used as starting material for the SALSA MLPA P041 and P042 *ATM* kits (MRC-Holland, Amsterdam, Netherlands, www.mrc-holland.com) [Schouten et al., 2002]. The P041 probe mix contained probes for 33 of the 65 exons as well as three probes for exon 1. The P042 *ATM* probe mix contained probes for the remaining *ATM* exons. Both probe mixtures also contained probes for control genes. After hybridization, ligation, and amplification, according to the instructions of the manufacturer, 1 μl of PCR product was mixed with 0.2 μl of ROX-500 labeled internal size standard, separated on an ABI Prism 3100 Avant automatic sequencer (Applera, Norwalk, Connecticut, CA), and analyzed using the GeneScan software ver.3.1. For MLPA data analysis, we used Coffalyser MLPA DAT software developed by MRC-Holland. For each probe, a range from 1 ± 0.2 was considered as a normal exon dosage, while a deletion was determined as being between 0.3 and 0.7.

Antisense Morpholino Oligonucleotide (AMO) Design and Treatment

A 25-mer antisense morpholino oligonucleotide (AMO) was designed to target the 5′ aberrant splice site of a pseudoexon mutation in pre-mRNA of JPAT11/12. The AMO-J11 sequence was: CCTGGAAAAATACTTACAATTAAAC. AMO748C (ATTCACACACTCGAATTCGAAAGTT) and AMO4956GC (CTTGGATAACTGCAACAAATTGACA) were designed to target wild-type sequences to determine potential regulatory elements at the site of a mutation(s). AMOs were synthesized by Gene-Tools (Philomath, OR). Treatment of LCLs with AMOs was performed as previously described [Du et al., 2007]. Cells were suspended in 5% FBS/RPMI medium and the AMO was added directly to medium at the concentrations indicated. Endo-Porter (Gene-Tools) was added to the medium to assist in intracellular incorporation of the AMO. Cells were collected after 48 hr for RNA analysis, and after 84 hr for ATM protein detection. Vivo-AMO was also used to treat JPAT 11 to enhance cellular delivery (Gene-Tools).

Irradiation Induced ATM-Ser1981 Foci Formation (IRIF)

Immunostaining of nuclear foci of ATM-Ser1981was performed as described [Du et al., 2007, 2009]. In brief, LCLs were first treated with the relevant compounds for 4 days before being irradiated with 2 Gy and then incubated at 37°C for 30 min. Next, the cells were fixed with 4% paraformaldehyde and then permeabilized on cover slips. The cover slips were blocked for 1 hr and incubated with mouse anti-ATM pSer1981 for 1 hr (1:500; Cell Signaling Technology, Danvers, MA). After a second blocking, cells were stained with Alexa Fluor 488 anti-mouse IgG (1:150; Invitrogen) for 1 hr and mounted onto slides.

Flow Cytometry Analysis of ATM-Ser1981 Autophosphorylation (FC-ATM-pSer1981)

FC-ATM-pSer1981 was used to verify the restoration of Ser1981 autophosphorylation by readthrough compounds (RTCs) [Du et al., 2009; Nahas et al., 2009]. The cells were treated for 4 days with RTCs, resuspended in PBS, and irradiated with 10 Gy. After 1 hr, the cells were fixed and permeabilized using FIX & PERM (Invitrogen). The cells were then incubated with 1 μl of mouse ATM-s1981 antibody (Cell Signaling Technology) for 2 hr at room temperature. After this time, cells were washed and resuspended in 100-μl PBS with Alexa Fluor 488 anti-mouse IgG (Invitrogen) for 45 min, and then washed and resuspended in PBS with 0.2% paraformaldehyde, before being analyzed using a FACSCalibur (BD, Franklin Lakes, NJ).

Western Blotting

Nuclear extracts were prepared by following the NE-PER protocol (Thermo Fisher Scientific, Rockford, IL). Proteins were separated on a 7.5% SDS-polyacrylamide gel. Western blots were prepared as described [Du et al., 2007], and probed with anti-ATM (Novus Biologicals, Littleton, CO), -SMC1, or -KAP1 antibodies (Novus Biologicals).

Results

Mutation Analysis

We initially screened our A-T patients for two previously reported Japanese mutations, c.4776(IVS33)+2T>A and c.7883_7887delTTATA [Ejima and Sasaki 1998; Fukao et al., 1998]. Neither of these mutations was detected.

STR genotyping of the *ATM* genomic region was performed for 11 JPAT patients, but since parental gDNAs were unavailable, we could only verify that one patient was homozygous for all markers (JPAT2): [S1819, 131; NS22, 165; S2179, 143; S1818, 162] [Mitui et al., 2003]. As a result, we set out to directly sequence the entire *ATM* coding region after PCR amplifying eight partially overlapping fragments from patients' cDNA [Du et al., 2008]. We identified 12 of the 16 expected mutations (75%) and confirmed them upon sequencing gDNA (Table 1). Only one patient (JPAT2) was homozygous, suggesting that most JPAT patients do not result from consanguineous marriages. The 12 mutations included four frameshifts (counting the homozygous JPAT2 twice), two nonsense, and six splice variants (Table 1). The remaining mutations (4/16; 25%) were four LGDs, which we identified after performing long-range PCR using gDNA as template. Fourteen mutations were novel; two had been previously reported: c.748C>T in JPAT6 [Teraoka et al., 1999] and c.2639-384A>G in JPAT11/12 [Sobeck 2001]. All mutations resulted in the absence of ATM protein (Supp. Fig. S1 and data not shown).

Splicing Mutations

The six splicing mutations identified were analyzed by using Maximum Entropy software (MaxENT) to estimate the strength of the splice sites [Yeo and Burge, 2004] and type of splice defect [Eng et al., 2004]. The mutations found are described below, and diagrams for potential splicing mechanisms are shown in Figure 1.

(1) c.331+5G>A (IVS6): This mutation changed the MaxENT score of the 5′ ss from 9.8 to 3.6. A shorter PCR product compatible with exon 6 skipping was observed at the cDNA level in patient JPAT1 using primers for exons 4 and 7 (Figs. 1 and 2A, lane 3).

(2) c.748C>T: cDNA from patient JPAT6 showed skipping of exon 9 (Figs. 1and 2B, lane 5). This allele with substitution c.748C>T predicted an amino acid change from Arg to a stop codon (CGA >TGA). Given that c.748C>T did not affect the scores for consensus splice sites, nor affect an ESE site, we hypothesized that it affected an as yet unknown splicing regulatory element. To test this idea further, we designed an AMO targeting the wild-type sequence at the site of the mutation in order to block the interaction between any regulatory molecule(s) and the wild-type sequence. Wild-type cells treated with increasing concentrations of AMO748C (Fig. 2G) showed skipping of exon 9, supporting idea model that the region around nucleotide 748 most likely contains a regulatory splicing motif.

(3) c.2639-384A>G (IVS19): The c.2639-384A>G variant in patient JPAT11/12 creates a novel splice acceptor site within IVS19 (Fig. 1), thereby creating a cryptic splice and "pseudoexon" of 58 bp is created in intron 19 (Fig. 2C, lanes 5 and 6).

Table 1. Mutations of Eight Japanese Families

Ex/Int	Patient	cDNA change	Genomic DNA mutation	Consequence
IVS6	JPAT1[a]	c.186_331del146 (deletes exon 6)	**c.331+5G>A (5′ss 9.81>3.58)**	Aberrant splicing (IV)
7	JPAT6[a]	c.397_398insT	**c.397_398insT**	Frameshift
9	JPAT6[b]	c.663_901del239 (deletes exon 9)	c.748C>T (R>X)	Aberrant splicing (III)
10	JPAT8/9[a]	c.902_1065del164 (deletes exon 10)	**c.902-19_1065+869del1052**	Large genomic deletion
IVS19	JPAT11/12[a]	c.2639_2640ins58	c.2639-384A>G (5′ss 0.36>8.54)	Aberrant splicing (II)
IVS19	JPAT3[a]	c.2639_2838del200 (deletes exon 20)	**c.2639-19_2639-7del13 (3′ss 8.8>3.4)**	Aberrant splicing (IV)
20	JPAT8/9[b]	c.2877C>G	**c.2877C>G (Y>X)**	Nonsense (TAG)
35	JPAT4/5[a]	c.4910_5005del96 (deletes exon 35)	**c.4956GC>TT (LQ>FX)**	Aberrant splicing (III)
38	JPAT1[b]	c.5415G>A	**c.5415G>A (W>X)**	Nonsense (TGA)
IVS48	JPAT11/12[b]	c.6808_7515del708 (deletes ex 49-52)	**c.6807+272_7516-275del5350**	Large genomic deletion
55	JPAT4/5[b]	c.7925_7926del2(GA)	**c.7925delGA**	Frameshift
60	JPAT10[a]	c.8419_8584del166 (deletes exon 60)	**c.8419-643_8507del732**	Large genomic deletion
61	JPAT10[b]	c.8585_8671del87 (deletes exon 61)	**c.8585-1G>C (5′ss 10.2>2.0)**	Aberrant splicing (IV)
61	JPAT2[h]	c.8624delA	**c.8624delA**	Frameshift
IVS63	JPAT3[b]	c.8851_9697del847	**c.8852-2kbdel17kb (CRAT [B] mutation?)**	Large genomic deletion

Bolded mutations have not been reported previously.
[a]First allele.
[b]Second allele.
[h]Homozygote.
Nucleotide numbering is based on +1 being the A of the first translation start codon in exon 4 (NCBI reference sequence: NM_000051.3).

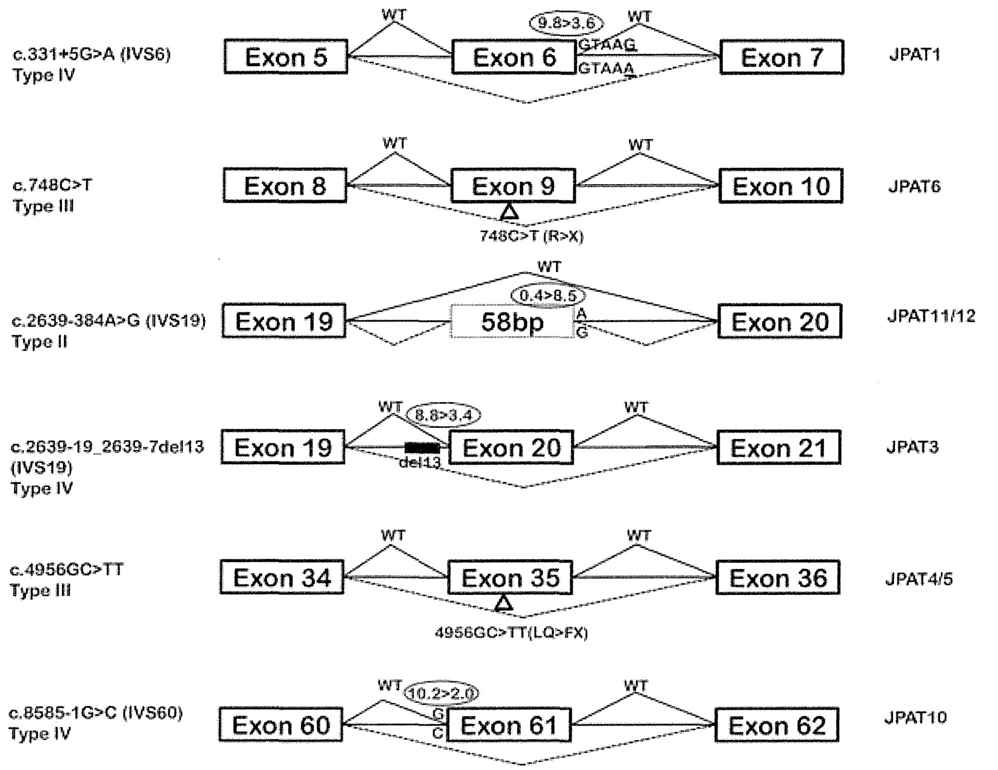

Figure 1. *ATM* splicing mutations. Genomic mutations causing splicing mutations were analyzed for changes in splicing scores calculated by Max ENT. Classification of splicing mutations is reported accordingly to Eng et al. [2004]. See text for additional details.

This results in a frameshift and a predicted secondary premature stop codon.

(4) c.2639-19_2639-7del13 (IVS19): In Figure 2D (lane 3), the PCR products from JPAT3 cDNA showed a normal and an additional prominent lower band (783 bp and 583 bp, respectively). Sequencing of the 583-bp band revealed skipping of exon 20. gDNA sequencing identified a 13 nt deletion in intron 19 at position c.2639-19_2639-7. The 3′ MaxENT score changed from 8.8 to 3.4 (Fig. 1).

(5) c.4956GC>TT: In family JPAT4/5, we identified a c.4956GC>TT substitution within exon 35 (p.LQ1652_1653FX) that leads to skipping of exon 35 without affecting an ESE or canonical splice sites (Figs. 1 and 2E, lanes 3 and 4). Exposing wild-type LCLs to increasing concentrations of AMO4956GC, targeting the mutation site, revealed skipping of exon 35 (Fig. 2H); these results suggest that nucleotide 4956 is part of a regulatory protein binding site, which when disrupted influences the aberrant splicing observed in JPAT4/5.

(6) c.8585-1G>C (IVS60): JPAT10 harbors the IVS60-1G>C mutation that changed the MaxENT score of the 3′ ss from 10.2 to 2.0, resulting in a skipping of the exon 61 (Fig. 2F, lane 4). Interestingly, the second allele of this patient was a splicing mutation that is predicted to result in exon 60 skipping (Fig. 2F, lane 4). We sequenced gDNA for exons 59–62 but failed to find a mutation that would account for the skipping of exon 60 (however, see additional results on JPAT10 below).

Large Genomic Deletions (LGDs)

(1) c.902-19_1065+869del1052 (del ex10): Two siblings (JPAT8/9) yielded an abnormal 369-bp fragment when cDNA was amplified from exon 9 to 11 (Fig. 3A, cDNA gel, lanes 3 and 4). When this band was isolated and sequenced, we found a deletion of exon 10. No mutation was observed in exons 9–11, ruling out a conventional splicing mutation. Using long-range PCR to amplify the genomic region from exon 9 to 11, we obtained a 3.3 kb fragment (Fig. 3A, gDNA gel lanes 3 and 4), whose sequence revealed a 1,052-bp deletion from IVS9-19 to IVS10+869; this deletion included exon 10 (164 bp).

(2) c.6807+272_7516-275del5350 (del ex49-52): Two siblings (JPAT11/12) showed an abnormal PCR fragment of 1.1 kb when cDNA was amplified from exon 48 to 53 (Fig. 3B, cDNA gel). The sequence of the PCR product showed a deletion of exons 49–52. A long-range PCR performed on gDNA using primers for exons 48 and 53 produced a 1.1 kb band instead of the expected 6.4 kb (Fig. 3B, left). Sequencing of the 1.1 kb band revealed a 5,350-bp genomic deletion that starts in intron 48 and ends in intron 52.

(3) c.8419-643_8507del732 (del ex 60): In patient JPAT10, we suspected that skipping of exon 60 might reflect an LGD. We amplified the gDNA surrounding exons 59–61 and found a 732-bp genomic deletion extending from IVS59-643 to nucleotide 89 of exon 60 (Fig. 3C).

(4) c.8851-2kbdel17kb (del ex64-65): When mutation screening failed to identify a second pathogenic mutation in JPAT3, we were prompted to search for an LGD mutation with Multiplex Ligation-dependent Probe Amplification (MLPA). We observed a significant decrease in peak height for the final exons 64 and 65, indicative of a deletion carried in heterozygous state (Fig. 4A). Previous studies have demonstrated two LINE-1 sequences between IVS63 and downstream of exon 65, as well as a 17 kb genomic deletion in the *ATM* gene of A-T patients

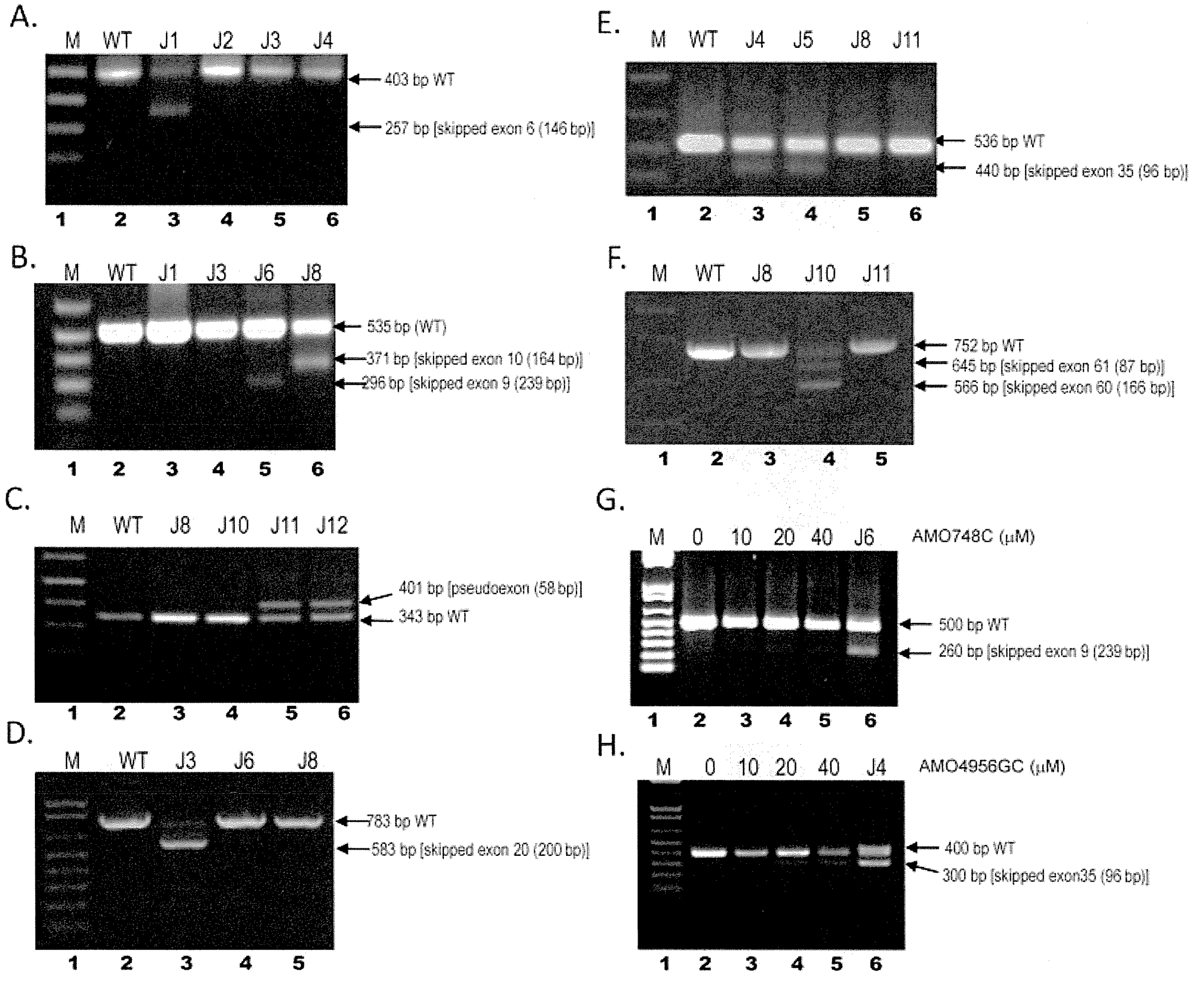

Figure 2. Effect of splicing mutations on cDNA. Agarose gel images of PCR products showed aberrant spliced products. Patient cDNA were used as templates for PCR amplifications in the regions displaying splicing mutations. M (lane 1) is 1 kb plus ladder (Invitrogen), wild-type cDNA was used as control (lane 2). **(A)** Skipped exon 6 in JPAT1 (lane 3). **(B)** Skipped exon 9 in JPAT6 (lane 5) and skipped exon 10 in JPAT8 (lane 6). **(C)** Pseudoexon of JPAT11 and JPAT12 (lanes 5 and 6). **(D)** Skipped exon 20 in JPAT3 (lane 3). **(E)** Skipped exon 35 in JPAT4 and JPAT5 (lanes 3 and 4). **(F)** Skipped exons 60 and 61 in JPAT10 (lane 4). **(G)** AMO-treated wild-type lymphoblastoid cell line (LCL) produced alternative spliced product that skipped exon 9. JPAT6, carrying the c.748C>T mutation, showed a skipped exon 9 product (lane 6), **(H)** AMO 4956GC treated wild-type LCL produced alternative spliced product that skipped exon 35. JPAT4 that has 4956GC>TT mutation showing skipped exon 35 products as a control (lane 6). See text for additional details.

with Costa Rican, Dutch, and Brazilian backgrounds [Broeks et al., 1998; Coutinho et al., 2004; Mitui et al., 2003; Telatar et al., 1998b].

Figure 4B summarizes the locations of primers, LINE-1 sequences, and an LGD for this region.

We used two sets of primers: Primer set #1 (P1Fw and P4Rev) was 23 kb apart, flanking the 17 kb deletion. Because of the nature of our PCR conditions, no PCR product was anticipated from the wild-type allele, while the mutant allele should yield a 6 kb fragment. Primer set #2 (P2Fw and P3Rev) was placed within the 17 kb deletion, which should have produced a 2.4 kb fragment from only the wild-type allele [Telatar et al., 1998b]. Figure 4B (lane 2) shows that wild-type gDNA produced the 2.4 kb fragment, while CRAT [B] (a Costa Rican patient homozygous for a 17 kb deletion) produced the 6 kb fragment (lane 4). A CRAT [B] heterozygote produced both the 2.4 kb fragment and the 6 kb product from the deletion (Fig. 4B, lane 5). The CRAT [B] band pattern was also observed in the gDNA of JPAT3, suggesting the presence of an LGD between two LINE-1 sequences (Fig. 4B, lane 3). Available breakpoints and surrounding sequences were analyzed using Repeat Masker software to search for flanking repetitive elements [Babushok and Kazazian, 2007; Kazazian and Goodier, 2002; Telatar et al., 1998b] (see Fig. 3). Because the breakpoint was in a highly homologous repeat sequence, the ends could not be accurately determined. The other Japanese patient (JPAT8) who did not have a deletion in this region showed a pattern identical to the wild type (Fig. 4B, lane 6).

The STR haplotypes for JPAT3, CRAT [B], and BRAT3 differed. JPAT3: S1819 [131,133]; NS22 [173,175]; S2179 [137,137]; S1818 [160,168]; CRAT [B]: S1819 [131]; NS22 [171]; S2179 [141]; S1818 [160] [Mitui et al., 2003]; BRAT 3: S1819 [133]; NS22 [155]; S2179

Figure 3

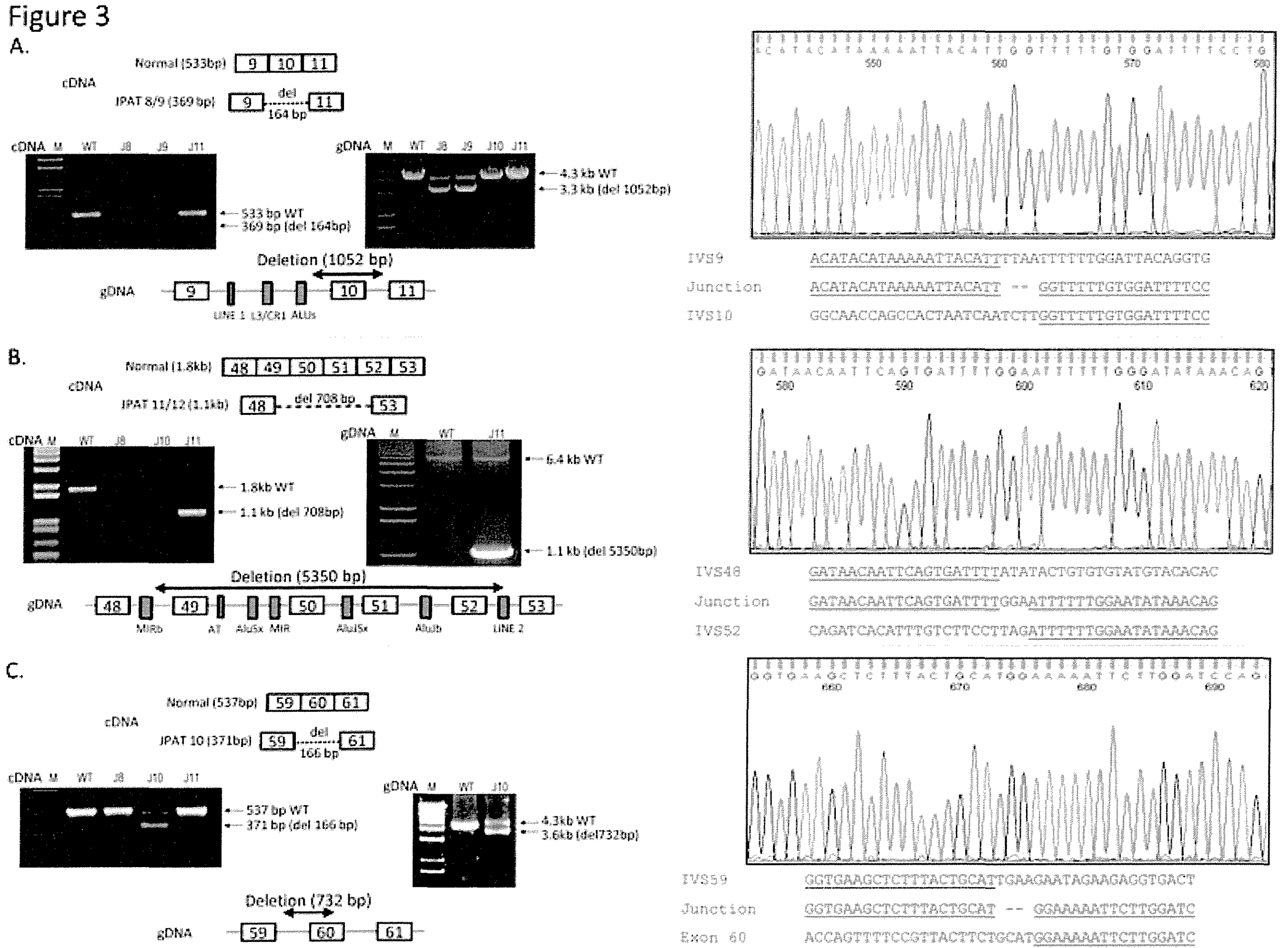

Figure 3. Large genomic deletions (LGDs). **(A)** Schematic representation of cDNA showing deletion of exon 10 and agarose gel image of PCR products (using primers GFw and GRev) (left): Lane 1 is 1 kb plus ladder (Invitrogen), lane 2 is wild-type control, lane 3 (JPAT8) and lane 4 (JPAT9) showing deletion of exon 10, lane 5 is JPAT control. Agarose gel image (right) for genomic DNA (gDNA) PCR products (using primers EX9Fw and EX11Rev) showing deletion of 1 kb in JPAT8/9. Schematic representation of DNA shows LGD, as well as repetitive elements within the region (at bottom). Sequence data with junction sequences are shown on right. **(B)** Schematic representation of cDNA change in JPAT11/12 between exon 48 and exon 53, which are analyzed by PCR (using primers FATFw and FATRev). Agarose gel image (left) for cDNA shows aberrant spliced products of JPAT11 (lane 5). Lane 1 is 1 kb plus ladder, lane 2 is wild-type, lanes 3 and 4 are JPAT control. Agarose gel image (right) for gDNA shows deletion of 5.3 kb (using EX Taq polymerase with LREX48Fw and LREX53Rev primers). Schematic representation of gDNA (at bottom) shows large deletion. Sequence data with junction sequences are shown on right. **(C)** Schematic representation of JPAT10 cDNA shows deletion of exon 60. Agarose gel image (left) shows aberrant spliced products. Agarose gel image (right) for gDNA PCR products (using primers EX59Fw and EX61Rev) show reduced size in JPAT10 (3.6 kb) compared to wild type (4.3 kb) and schematic representation of gDNA showing deletion at c.8269-643del732, which includes the first 89 bp of exon 60. Sequences are shown at right.

[147]; S1818 [146] [Mitui et al., 2003]. These results suggested that the c.8851-2kbdel17kb mutations in the three patients were not ancestrally related.

Correction of Type II Pseudoexon Splicing Mutation using an AMO

In family JPAT11/12, we identified a type II splicing mutation [Eng et al., 2004] c.2639-384A>G, which created a cryptic acceptor splice site resulting in the inclusion of 58 bp of intronic sequence (Figs. 2C and 5A). We designed AMO-J11 to target the cryptic 5′ splice site (Fig. 5A) [Du et al., 2007; Eng et al., 2004]. The LCL of JPAT11 was treated with AMO-J11 for 4 days followed by RT-PCR analysis. Mutant splicing was almost completely abrogated in an AMO dose-dependent manner and normal transcript was restored (Fig. 5B). Nuclear extracts from treated JPAT11 cells also showed a full-length ATM protein (data not shown). In order to enhance the delivery and efficiency of the AMO, we also designed a structurally modified AMO referred as "Vivo-AMO" [Morcos et al., 2008; Moulton and Jiang, 2009]. Notably, a significant amount of functional ATM protein was induced by 0.5 μM Vivo AMO-J11 (Fig. 5C). However, "Vivo-AMO" started to show possible cytotoxicity at 0.8μM (Fig. 5C, lane 4).

Correction of Nonsense Mutation in JPAT8 using RTCs

The JPAT8/9 siblings lack ATM protein because they carry an LGD and a nonsense mutation (c.2877C>G, p.Tyr959X). Functional ATM protein is inducible with compounds that readthrough premature termination codons [Du et al., 2009] even when the LCL carries the nonsense mutation in a heterozygous state [Lai et al., 2004]. We treated JPAT8 LCL with the readthrough compound RTC13 for 4